Lectures on Dynamics of Dark Matter: Linear and Non-linear Effects

J. A. de Freitas Pacheco
Universidade Federal do Espirito Santo - Vitoria
University of Nice-Sophia Antipolis – Observatoire de la Côte d'Azur

1. Introduction

In our days, the comprehension of the nature of dark matter is one of the greatest challenges for physicists and astrophysicists. Gravitational effects at different scales suggest the presence of some unknown form of matter in the universe, corresponding to an amount of about 23% of the so-called critical density ($\rho_{crit} = 3H_0^2/8\pi G = 1.89\times10^{-29}h^2\ gcm^{-3}$, where h is the present value of the Hubble parameter in units of 100 km/s/Mpc). In fact, the abundance of elements like ^{2}H, ^{4}He, ^{3}He and ^{7}Li, "cooked" in the early phases of the universe, depends essentially on the baryon-to-photon ratio η. For a universe evolving adiabatically, such a ratio remains constant and the observed abundance of the primordial elements permits to estimate the ratio η. Since the present relic photon density is known (about 410 cm^{-3}), the baryon density can be computed. The resulting value corresponds to about 4% of the critical density, indicating clearly that baryons under any form (stars, cold or hot gas) cannot explain the gravitational effects (which will be analyzed later) observed in scale of galaxies, groups and clusters.

The only particle of the standard model having abundance large enough to explain the observations is the neutrino (density of about 112 cm^{-3} per flavor). In this case, in order to satisfy the constraint of a cosmic mass density of about 23%, the average mass of the different neutrino flavors should be of the order of 4.3 eV. In fact, neutrino oscillation experiments, which measure mass squared differences (see, King, arXiv:0712.1750 for a review) suggest lower values. If considered as a Majorana particle, the Heidelberg-Moscow experiment (whose data analysis is contested by some other experimentalists) on double β-decay of ^{76}Ge, indicate a mass of 0.33±0.22 eV, one order of magnitude less than that required to explain the "observed" amount of dark matter. In reality, there is another difficulty with the neutrino as a dark matter candidate. Neutrinos decouple relativistically and if they had a mass of 1.0 eV, they stream freely until the period of matter-radiation equality (z ~ 3300) up to distances of about 14 Mpc , corresponding to a mass scale of about 4×10^{14} $M_\odot$. Thus, neutrinos erase all fluctuations in the galactic scale, favoring an up-down scenario of structure formation.

The absence of relic candidates of the standard model pushed physicists to examine extensions of that model. In particular, models including supersymmetry (SUSY), lead to new candidates like s-neutrinos, gravitinos or photinos among others. Presently, the most plausible candidate is the neutralino χ, which is the lightest supersymmetric particle. However, there is an embarrassing problem: up to now, no signal of supersymmetry has been seen in the Large Hadron Collider (LHC) of CERN. The decay of B-mesons (including $b\bar{b}$ quarks) shows no indication of "exotic" particles like the chargino or the neutralino. The situation is more delicate when direct search experiments are considered. In these experiments, a DM particle collides elastically with a nucleus, which suffers recoil and dissipates energy that is measured by the detector. The orbital velocity of the Earth combines with that of the Sun around the galactic center and, consequently, a modulation of the signal amplitude with a period of one year should be seen. In fact, this has been claimed for more than one decade by the team of the experiment DAMA/LIBRA and now there are indications that a similar signal has been also detected by the experiments CoGeNT and CRESS-II (Kelso et al., arXiv:1110.5338; Arina et al., arXiv:1111.3238; Hooper, arXiv:1201.1303). However, these findings are not confirmed by the more sensitive experiment XENON100 (Aprile et al., arXiv:1005.0380).

The recent claim by two experiments (ATLAS and CMS) running at CERN, that a signal at the energy of about 125 GeV could be associated to the Higgs boson, permits to restrict better the mass range of dark matter particles. This value, introduced in SUGRA models and combined with the upper limits on the dark matter particle-nucleon cross section derived from XENON100 and the dark matter abundance derived from the seven years WMAP data, constrain the mass of the lightest particle of the "Minimal Supersymmetric Model" (MSSM) to be $\boldsymbol{m_\chi} > 160$ GeV (Beskidt et al., arXiv:1202.3366; Baer et al., PRD 85, 075010, 2012; Akula et al., PRD 85, 075001, 2012). Interestingly, the non-detection of gamma rays originated from the $\chi\bar{\chi}$ annihilation in the center of M87, either at energies of 100 MeV or 1 GeV by FERMI-LAT, implies also that $\boldsymbol{m_\chi} > 100$ GeV (Peirani et al., PRD 70, 043503, 2004). On the other hand, there are recent claims concerning the detection of a gamma ray line at ~ 130 GeV from the galactic center (Tempel et al., arXiv:1205.1045; Su & Finkbeiner, arXiv:1206.1616) and from several clusters of galaxies (Hektor et al., arXiv:1207.4466) in FERMI-LAT data. Gamma-ray lines can be produced during the annihilation of dark matter particles through two channels: either by two-photon emission by the reaction $\chi\bar{\chi} \to \gamma\gamma$ or by a single photon emission by the reaction $\chi\bar{\chi} \to Z^0\gamma$ (Peirani & de Freitas Pacheco, arXiv:0503380). In the former, the photon energy is $\varepsilon_\gamma \approx m_\chi$, whereas in the latter the photon energy is given by $\varepsilon_\gamma = (m_\chi - m_{Z^0}^2 / 4m_\chi)$. For a photon energy of 130 GeV, the corresponding neutralino masses are 130 GeV and 144 GeV for the first and the second channel respectively, consistent with the constraints mentioned previously. A different origin for this possible γ-ray line was proposed by Bergstrom (arXiv:1208.6082), who assumed the existence of right-handed neutrinos having a mass of about 135 GeV. According to his calculations, the FERMI-LAT feature at 130 GeV can be quite well explained by the following processes: i) broad internal bremsstrahlung ($\nu_R\nu_R \to \ell^+\ell^-\gamma$), producing a bump around 120 GeV; ii) a two-photon line at 135 GeV issued from the process $\nu_R\nu_R \to 2\gamma$ and finally, iii) a γ-line around 119.6 GeV resulting from the process $\nu_R\nu_R \to Z\gamma$. Further observations must decide about the reality of such a feature and its true origin.

Although the DM theory predicts correctly different aspects of the large structure of the universe and, in particular, the formation of galaxies, some problems persist. Cosmological simulations predict too much dark matter at the center of galaxies and a large number of satellites, which are not observed. Different issues to these problems have been proposed. Some of them are quite drastic, since they claim a failure of General Relativity at cosmological scales, requiring alternative gravitational theories.

In these lectures, it is assumed that dark matter is a reality (thus, General Relativity is a "good" theory) and constituted by weakly interacting particles not issued from the standard model. In the following sections the evidence for the existence of dark matter in different scales is reviewed as well as its dynamical behavior at different evolutionary phases of the universe.

II. Evidence of Dark Matter in the Universe

II.1 Clusters of galaxies

Historically, since 1933 the presence of "non-luminous" matter in a gravitational system was suspected by the Swiss astronomer Fritz Zwicky. He noticed that the mean velocity of galaxies in the Coma cluster was too high for the measured (total) luminosity, under the assumption that the system was in dynamical equilibrium. Zwicky assumed a certain relation between the mass and the luminosity for the galaxies of the cluster and the virial relation to compute the expected mean galaxian velocity that was lower than the observed value.

As we will see, the basic assumption involved in mass estimates of astronomical systems is that of ***dynamical equilibrium***. Most authors consider that Coma is the archetype of a "relaxed" cluster, an idea based mainly on its quasi-spherical morphology. However, substructures have been identified in the cluster (Escalera et al., A&A 264, 379, 1992), weakening this argument. Even so, let us assume that the cluster is relaxed and that galaxies track the ***total*** gravitational potential. For a spherical system in which the 1D-velocity dispersion is constant, using the Jeans equation (the derivation of this equation will be discussed later) the total mass inside the radius *R* is

$$M(\leq R) = -\frac{\sigma_r^2 R}{G}\left(\frac{\partial \lg n(r)}{\partial \lg r}\right)_R \qquad \text{II.1.1}$$

where n(r) is the density of galaxies. This quantity can be obtained by inversion of an Abel integral involving the projected density of galaxies $\Sigma(a)$ at a given projected distance *"a"* from the center, an observed quantity. Figure 1 shows the projected density of galaxies derived from Zwicky counts.

The de-projected density of galaxies is given by

$$n(r) = -\frac{1}{\pi}\int_r^\infty \frac{\partial \Sigma(a)}{\partial a}\frac{da}{\sqrt{a^2 - r^2}} \qquad \text{II.1.2}$$

Combining eqs. II.1.2 and II.1.1 and using $\sigma_r = 1008\ kms^{-1}$, one obtains for the total mass inside *R = 2.5 Mpc* the value $M = 1.48 \times 10^{15}$ $M_\odot$. Since the luminosity of the cluster is about L_B = 1.0x10^{13} $L_\odot$, the corresponding mass-to-luminosity ratio is $M / L_B \approx 148$ (in solar units), indicating a substantial amount of non-baryonic matter in the cluster (It should be mentioned that the mass-to-luminosity ratio in the B filter varies from 4 for spiral galaxies up to 8 for elliptical ones). From the derivative of equation II.1.1, one obtains for the central DM density a value of 2.9 $M_\odot pc^{-3}$.

Figure 1
Projected galaxy density as a function of the radial distance. Data from Zwicky and solid (red) curve represents a polynomial fit.

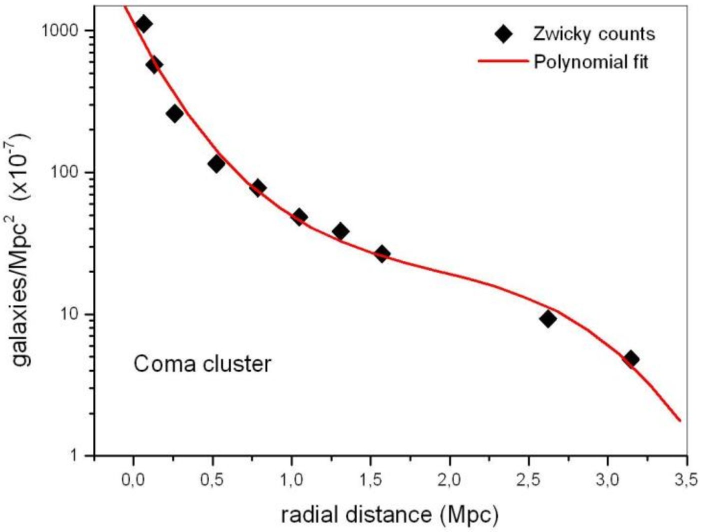

Galaxies are not the only tracer of the potential. Hot gas, detected by its X-ray emission can also be used to track dark matter. If the hot intra-cluster gas is in hydrostatic equilibrium and has a uniform temperature distribution, then the total mass inside a radius *R* is given by

$$M(\leq R) = -\frac{kT}{\mu m_p}\frac{R}{G}\left(\frac{\partial \lg n_{gas}}{\partial \lg r}\right)_R \qquad \text{II.1.3}$$

where μ is the mean molecular weight, m_p is the proton mass and n_{gas} is the hot gas particle density. Combining eqs. II.1.1 and II.1.3 gives $n_{gas} \propto n^{\beta}$ where $\beta = (\mu m_p / kT)\sigma_r^2$. These last relations define the so-called "β-model" for the intra-cluster gas. Using the following ansatz for the density profile of the hot gas

$$n_{gas}(r) = n_0 / \left[1 + \left(\frac{r}{r_c}\right)^2\right]^{\beta} \qquad \text{II.1.4}$$

one obtains for the X-ray brightness distribution (remember that the emissivity due to bremsstrahlung is proportional to the square of the gas density)

$$S(a) = S_0 / \left[1 + \left(\frac{a}{r_c}\right)^2\right]^{2\beta - 1/2} \qquad \text{II.1.5}$$

In the above equations, n_0 is the central gas density, r_c is the "core" radius, S_0 is the central X-ray brightness and *a* is the projected distance to the center of the cluster.

Let us take as an example the cluster A1795. The X-ray data from ***Chandra*** (see Figure 2) can be fitted by eq. II.1.5, permitting an estimation of the parameters β, r_c and S_0. Then, the parameters β and r_c can be inserted into eq.II.1.4, which permits to compute the total mass from eq.II.1.3. The measured average temperature of the hot gas is 4.0 KeV, the resulting mass inside a radius of 2.0 Mpc is 5.7×10^{14} $M_{\odot}$ and the central DM density is about 0.035 $M_{\odot}pc^{-3}$. Again, when compared with the mass of baryons under the form of hot gas and under the form of stars, we conclude that a substantial amount is "dark", i.e., not seen in visible light or in X-rays.

Figure 2
X-ray brightness profile of A1795

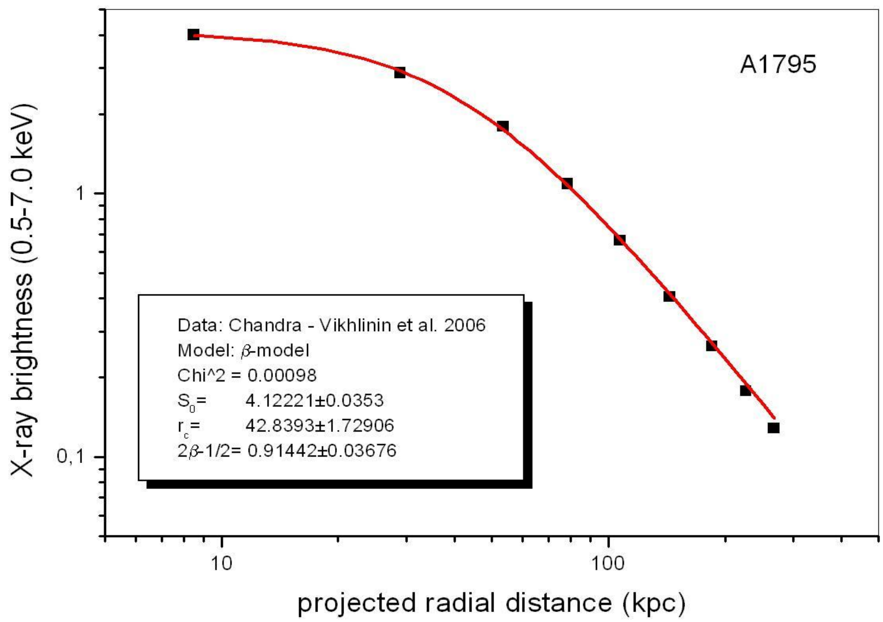

II.2 Groups of Galaxies

If clusters permit to probe the presence of dark matter in scales of 1-2 Mpc, groups of galaxies, including a few tens of objects, permit to investigate dark matter effects at scales of 100-400 kpc. Groups are generally supposed to be in equilibrium in order that the virial be satisfied. Here we assume that this is not generally the case and that the global dynamics of the system is described by the Jacobi identity.

Supposing that the system is homogeneous, i.e., the density of galaxies is constant inside a fictitious spherical volume of radius *R*, the probability *P(a)* of finding a galaxy at a projected distance *a* from the center depends only of the effective depth at such a distance, i.e.,

$$P(a) = 2K \int_0^{\sqrt{R^2-a^2}} dz = 2K\sqrt{R^2-a^2} \qquad \text{II.2.1}$$

where $K = 3/4\pi R^3$ is a normalization constant such as

$$\int_0^R 2\pi a P(a) da = 1 \qquad \text{II.2.2}$$

Then, the mean projected distance, the mean inverse projected distance and the squared projected distance, which are the observable quantities, can be computed and they are given respectively by

$$\langle a \rangle = \frac{3\pi}{16} R \; ; \; \left\langle \frac{1}{a} \right\rangle = \frac{3\pi}{4R} \; ; \; \langle a^2 \rangle = \frac{12}{15} R^2 \qquad \text{II.2.3}$$

The Jacobi identity describing the dynamical state of the system is

$$\frac{1}{2}\frac{d^2 I}{dt^2} = 2T + W \qquad \text{II.2.4}$$

where I is the moment of inertia of the system, T is the kinetic energy and W is the gravitational potential energy. Notice that in dynamical equilibrium, the left side of eq. II.2.4 is null and the virial relation is recovered. Using the relations in II.2.3, the different terms of the Jacobi identity can be written as

$$W = -\frac{3}{5}\frac{GM^2}{R} = -\frac{4}{5\pi} GM^2 \left\langle \frac{1}{a} \right\rangle \qquad \text{II.2.5}$$

$$T = \frac{1}{2}\sum_i^N m_i v_i^2 = \frac{3}{2} M \sigma_z^2 \qquad \text{II.2.6}$$

and

$$I = \frac{3}{5} MR^2 = \frac{3}{4} M \langle a^2 \rangle \qquad \text{II.2.7}$$

An isotropic distribution of velocities was supposed when computing the kinetic energy. Now, make the approximation

$$\frac{1}{2}\frac{d^2 I}{dt^2} \approx \pm \frac{I}{2\tau^2} \approx \pm \frac{81\pi^2}{2048} \frac{\langle a^2 \rangle}{\langle a \rangle^2} M \sigma_z^2$$

where we have introduced the crossing time defined by

$$\tau = \frac{R}{\sqrt{3}\sigma_z} = \frac{16}{3\sqrt{3}\pi} \frac{\langle a \rangle}{\sigma_z}$$

Replacing all these relation into eq. II.2.4 and solving for the mass M one obtains

$$M = \frac{15\pi}{4G}\sigma_z^2 \left\langle \frac{1}{a} \right\rangle^{-1} \left[1 \pm \frac{27\pi^2 \langle a^2 \rangle}{2048 \langle a \rangle^2} \right] \qquad \text{II.2.8}$$

In the above equation, the positive sign corresponds to an expanding group while the negative sign indicates a contracting group.

As an example, consider the group NGC 383, constituted by 9 bright galaxies whose total luminosity is $L_B = 3.6 \times 10^{11}$ $L_{B,\odot}$. The velocity dispersion of galaxies is $\sigma_z = 504\, km/s$ and the different averages involving projected distances are: $\langle a \rangle = 105\, Kpc$; $\langle a^2 \rangle = 14167\, Kpc^2$; $\langle 1/a \rangle = 0.022\, Kpc^{-1}$. From these, we derived for the effective radius of the system *R = 178 Kpc* and, from eq. II.2.8, a mass $M = 3.14 \times 10^{13}(1 \pm 0.168)$ $M_\odot$. The group is probably is collapsing, so its probable mass is $M = 2.6 \times 10^{13}$ $M_{\odot,}$ implying a mass-to-luminosity ratio $M/L = 73$, which indicates again the presence of dark matter in the system.

II.3 Binary Galaxies

Binary galaxies represent an intermediate scale between clusters and groups at which dark matter can be probed. Typically, the separation of these interacting systems is in the range 50-80 kpc. One of the major difficulties to study these systems is that catalogs are often contaminated by "optical" pairs, i.e., galaxies that are not physically connected but are close only by projection effects. When tidal distortions are not seen in the morphology of the galaxies, it is difficult to conclude if a pair is real or "optical".

Here we follow the statistical approach by de Freitas Pacheco & Junqueira (Ap&SS 149, 141, 1988) to analyze a given sample of binaries. The observed quantities are the velocity difference in the line-of-sight V_z and the projected separation of the pair r_p. Introduce now the dynamical quantity $q = V_z^2 r_p$ .If the galaxies follow elliptical orbits, a simple exercise gives

$$q = G(M_1 + M_2)F(\theta, i, \varpi, e) \qquad \text{II.3.1}$$

where M_1, M_2 are the masses of the galaxies and the orbital function F depends on the phase angle θ, the inclination of the orbit i, the longitude of the periastron ϖ and on the eccentricity e. The orbital function is given explicitly by the equation

$$F = \frac{\sin^2 i \left(\sin\theta + e \sin\varpi\right)^2 \left(\cos^2\theta \cos^2 i + \sin^2\theta\right)^{1/2}}{\left[1 + e\cos\left(\theta - \varpi\right)\right]} \qquad \text{II.3.2}$$

We further assume that the total mass of the pair is proportional to its total luminosity, i.e., $M = fL$ and that the mass-to-luminosity ratio is the same for a given sample of pairs. Here we will discuss the analysis of a sample of 233 pairs prepared by Karachentsev. Under these conditions, from II.3.1, we can write for each member of the catalog

$$\log q_i = \log f + \log(GL_i F_i) \qquad \text{II.3.3}$$

Using a Monte Carlo procedure, the distribution of the quantity $\log(GLF)$ is calculated by assuming: i) a log-normal distribution for the luminosity whose parameters were obtained from the catalog data (median equal to $\log L_B = 10.80\,\mathrm{L}_\odot$ and dispersion equal to $\sigma_{\log L} = 0.53$); ii) the longitude of the periastron and the inclination of the orbit are random variables, varying uniformly in their domains of validity; iii) the orbits fill the phase space, thus the distribution probability of eccentricities is *P(e)de = 2ede* ; iv) for elliptical orbits, the distribution probability of the phase angle θ is

$$P(\theta)d\theta = \frac{(1-e^2)^{3/2}}{\left[1+e\cos(\theta-\varpi)\right]}d\theta \qquad \text{II.3.4}$$

On the other hand, the distribution of the quantity *log q* can be derived directly from the catalog data. The best fit of both distributions gives the mean mass-to-luminosity ratio *f* of the sample. This is shown in figure 3.

Figure 3
Simulated and observed distributions for binary systems

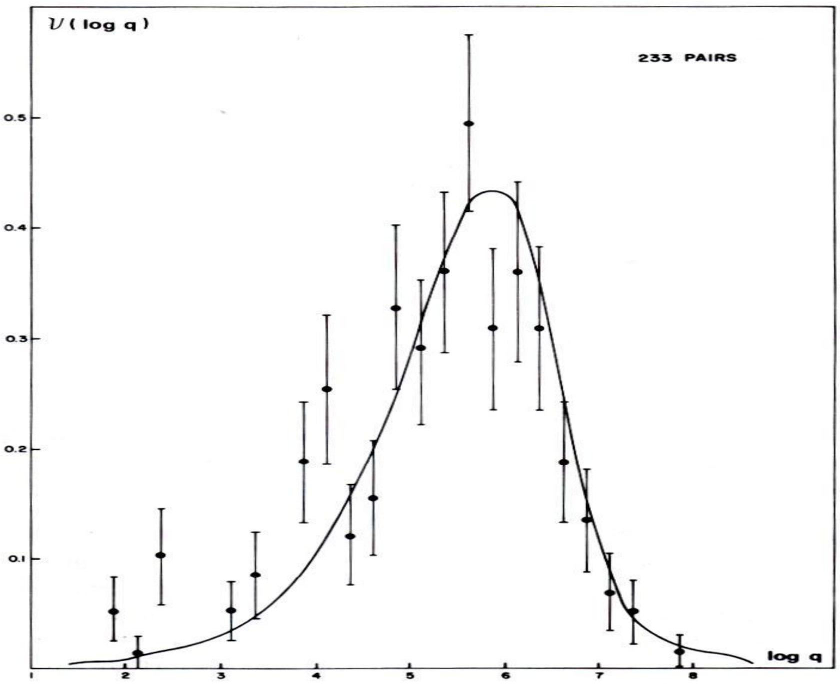

The best fit gives M/L = 25 while the expected value, taking into account that 80% of the galaxies in the catalog are early type is M/L = 5.6, which puts in evidence the presence of dark matter in scales of the order of 47 Kpc, the mean projected separation of the pairs.

II.4 Galaxies – Flat Rotation Curves

If light traces matter, the rotation curves of galaxies should decline for distances beyond 10-15 Kpc from the center. However, this is not the case because the large amount of data collected by Vera Rubin (and others) since the seventies indicate that most of galaxies have flat rotation curves.

Rotation curves are generally modeled by the following procedure. From the observed brightness profile, the mass density can be derived by inversion techniques and by assuming a constant (or variable) mass-to-light ratio. Once the density is known, the solution of the Poisson equation gives the potential that introduced into Jeans equations permits an evaluation of the velocity profile. Another strategy consists to adopt a self-consistent potential-density pair whose parameters are chosen in order to fit the brightness profile of the galaxy. The latter approach was adopted by Ortega & de Freitas Pacheco (AJ 106, 899, 1993) to describe the kinematics of Sc galaxies. Gas-rich spirals have the advantage that dark matter can be tracked not only by stellar motions but also by the gas (21cm line) that can be detected up to distances of about 25-30 Kpc from the center. The adopted potential-density pair is that derived by Satoh (PASJ 32, 41, 1980), which is free of singularities and given by the equations (in cylindrical coordinates)

$$\phi_S(r,z) = -\frac{GM_S}{\left\{r^2+z^2+a\left[a+2\left(z^2+b^2\right)^{1/2}\right]\right\}^{1/2}} \qquad \text{II.4.1}$$

and

$$\rho_S(r,z) = \frac{ab^2M_S}{4\pi}\frac{\left\{r^2+z^2+\left[a+3\left(z^2+b^2\right)^{1/2}\right]\left[a+2\left(z^2+b^2\right)^{1/2}\right]\right\}}{\left\{r^2+z^2+a\left[a+2\left(z^2+b^2\right)^{1/2}\right]\right\}^{5/2}\left(z^2+b^2\right)^{3/2}} \qquad \text{II.4.2}$$

In these equations M_S is the total mass of the stellar component, b and a are the scales characterizing the distribution of mass along the vertical and radial directions respectively. These constants are free parameters of the model. The dark halo is modeled by the potential-density pair describing a non-singular isothermal halo as given by Binney & Tremaine (Galactic Dynamics – Princeton University Press, 1988), i.e.,

$$\phi_h(r,z) = \frac{V_0^2}{2}\lg\left(r^2+z^2+R_c^2\right) \qquad \text{II.4.3}$$

and

$$\rho_h(r,z) = \frac{V_0^2}{4\pi G}\frac{\left(r^2+z^2+3R_c^2\right)}{\left(r^2+z^2+R_c^2\right)^2} \qquad \text{II.4.4.}$$

In these equations, V_0 (dimension of a velocity) and R_c, the core radius of the halo, are constants and free parameters of the model. While the parameters in the first potential-density pair are derived by fitting the light distribution, those in the second pair are derived by fitting the kinematics of the galaxy. The next step consists to solve the Jeans equation in cylindrical coordinates describing the motion of the stars, namely

$$\frac{\partial\left(\rho_s \sigma_r^2\right)}{\partial r}+\frac{\rho_s}{r}\left(\sigma_r^2-\sigma_\theta^2-\bar{V}^2\right)+\rho_s \frac{\partial\left(\phi_s+\phi_h\right)}{\partial r}=0 \qquad \text{II.4.5}$$

In the above equation σ_r and σ_θ are respectively the radial and the tangential velocity dispersions and $\bar{V}$ is the average tangential velocity of the stars. This should not be confounded with the circular velocity defined by

$$V_c^2=r\frac{\partial\left(\phi_s+\phi_h\right)}{\partial r} \qquad \text{II.4.6}$$

The so-called rotation "drift" expressing the difference between the average tangential velocity and the circular velocity is derived from eqs. II.4.5 and II.4.6, i.e.,

$$\bar{V}^2-V_c^2=(\sigma_r^2-\sigma_\theta^2)+\frac{r}{\rho_s}\frac{\partial\left(\rho_s \sigma_r^2\right)}{\partial r} \qquad \text{II.4.7}$$

For stars, the observed quantities are the average tangential velocity and the velocity dispersion (profiles either along the major or the minor axes) projected in the line-of-sight. Thus, to compare the solutions of the system of equations above, it is necessary to calculate the velocity components along the line-of-sight, weighted by the luminosity density (or, equivalently, by the mass density), i.e.,

$$\left\langle \bar{V}(y)\right\rangle=\frac{1}{\mu}\int_{-\infty}^{\infty}\frac{y}{r}\rho_s(r,z)\bar{V}(r,z)\sin i\,ds \qquad \text{II.4.8}$$

where the integral is performed along the line-of-sight, y is the projected distance to the center along the major (minor) axis, i is the inclination angle of the orbital plane with respect to the line of sight and

$$\mu=\int_{-\infty}^{\infty}\rho_s(r,z)ds \qquad \text{II.4.9}$$

is the projected mass density along the line-of-sight.

Contrary to the stars, which have a rotation "drift" as mentioned above, the gas is supposed to follow only a "Keplerian" motion, i.e., its velocity is equal to the local circular velocity.

Figure 4
Theoretical rotation curve for the stellar component of NGC 6503 compared with observational data

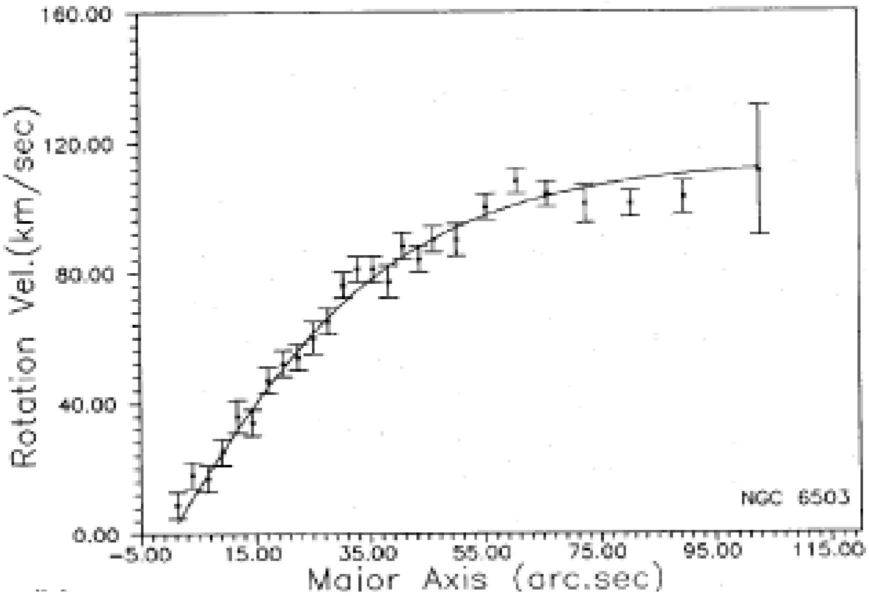

As an example of such a procedure, fig. 4 shows the rotation curve (average tangential velocity) computed for the Sc galaxy NGC 6503 (inclination angle $i = 74°$) compared with observational data. In fig. 5, the computed circular velocity is show in comparison with data derived from the 21cm line. Notice that the gas permits to probe the potential up to distances 8 times longer than the stellar component

Figure 5
Circular velocity compared with 21cm data for NCG 6503

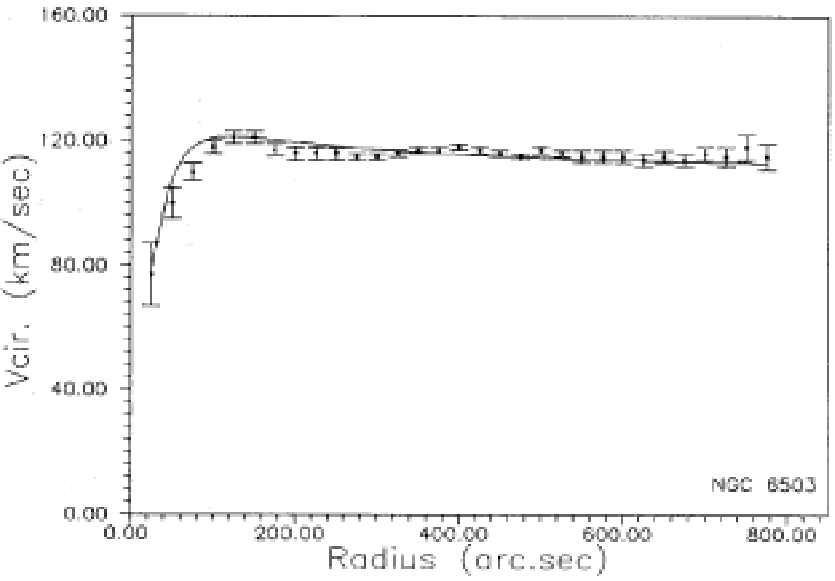

From the best fit of data, the following parameters for the potentials were derived: a = 1.2 Kpc; b/a = 0.1 and R_c = 1.4 Kpc. The central density of dark matter is $0.2\ M_{\odot}pc^{-3}$ while that of the baryonic component is one order of magnitude higher. The contribution of dark matter increases with the distance to the center and is dominant beyond 50 Kpc. A similar result was obtained for another Sc galaxy NGC 3198, whose potential parameters are: a = 2.0 Kpc; b/a = 0.1 and R_c = 4.0 Kpc. The central density of dark matter for this galaxy is lower than the precedent case, being only 0.045 $M_\odot pc^{-3}$ and the density of the baryonic component is about 40 times higher. These results indicate a general trend for late type galaxies – the central regions are dominated by the baryonic component and not by dark matter, contrary what cosmological simulations suggest, as it will be discussed later.

Another disturbing fact concerns the measurement of rotation velocities for 47 gas dominated galaxies (or Low Surface Brightness – LSB – objects) by McGaugh (PRL 106, 121303, 2011). For these objects, the baryonic mass is essentially under the form of gas and can be estimated more precisely than the stellar component. McGaugh found a robust correlation between the maximum rotation velocity and mass of the galaxy (supposed to be essentially the gaseous mass) of the form $M \propto V^4$. He claims that such a relation (Tully-Fisher relation) cannot be explained by the "canonical" ΛCDM model but it results naturally from MOND theory. We will return to this point latter.

In the case of elliptical galaxies, the presence of "hot coronae", seen in X-rays in a large number of massive early type objects, seem to require a dark matter halo to confine gravitationally the hot gas. The dynamical analysis of stellar rotation curves and velocity dispersion profiles by Ortega & de Freitas Pacheco (AJ 97, 1000, 1989) of a sample of these galaxies suggests that in about a half of the objects the M/L ratio increases slightly with radius, indicating the presence of dark matter. In other words, in early type galaxies dark matter manifests its presence only for distances larger than 15-20 Kpc. This conclusion seems to be supported by the investigation of Romanowsky et al. (Sci 301, 1696, 2003), who studied the rotation of E-galaxies using planetary nebulae as probes of the potential. They found little if any dark matter in the objects of their sample. More recently, Wegner et al. (arXiv:1206.5768) studied rotation curves of 8 E-galaxies in the A262 cluster and they found extremely low values for the mean halo density within the optical radius of the order of 0.02 $M_\odot pc^{-3}$. However, this picture is challenged by the results of Biressa & de Freitas Pacheco (Gen.Rel.&Grav. 43, 2649, 2011) who estimated the central dark matter density in three E-galaxies situated respectively at redshift 0.11, 0.48 and 0.94. These galaxies act as gravitational lenses, imaging distant quasars that display an almost circular image (Einstein "ring"). For these galaxies, the authors found an average central dark matter density of 0.55 $M_\odot pc^{-3}$, substantially higher than previous investigations. Is this result a characteristic of massive E-galaxies or simply a consequence of the evolutionary history of their halos? More data are required to elucidate this important question.

II.5 Dark Matter in the Solar Neighborhood

Already in the early thirties, the Dutch astronomer Jan Oort from the analysis of the stellar motions perpendicular to the galactic plane concluded that the dynamical mass density is about twice that obtained by adding the masses of the different stellar populations present in the solar neighborhood. This problem is quite similar to the situation found by Zwicky in the Coma cluster. The presence (or not) of dark matter in our vicinity is quite important since its density is a key factor for all direct detection experiments running in the world, mentioned before.

Here also the situation is highly controversial. In the sixties Oort (BAN 15, 45, 1960) revised his estimates of the dynamical mass density in the solar vicinity from which it is possible to derive a dark matter density of about $\rho_{\rm dm} \approx 0.05\ M_{\odot}pc^{-3}$. Crezé et al. (A&A 329, 920, 1998) using Hipparcos data found no evidence for dark matter in our neighborhood. A subsequent analysis by Holmberg & Flynn (MNRAS 313, 209, 2000) again based on Hipparcos data on A and F stars, leads to an estimated for the dynamical mass of $0.102 \pm 0.010\ M_{\odot}pc^{-3}$, which should be compared with the estimate for the "visible" mass of $0.095\ M_{\odot}pc^{-3}$. Thus, the authors concluded that taking into account the uncertainties, there is no compelling evidence for a significant amount of dark matter in the solar region. These "negative" results were reinforced by the recent investigation of Moni Bidin et al. (ApJ 751, 30, 2012) who analyzed the kinematics of 412 red giants in the thick disk, concluding that there is no robust evidence for dark matter in the disk near the Sun. However, Bovy & Tremaine (arXiv:1205.4033) contested the method of analysis by Moni Bidin et al., concluding for a dark matter density in the solar neighborhood of $\rho_{dm} = 0.008 \pm 0.002\ M_{\odot}pc^{-3}$. A still higher density was obtained by Garbari et al. (arXiv:1206.0015), who have analyzed a sample of 2000 K dwarves taken from the literature and found a dark matter density of $\rho_{dm} = 0.025 \pm 0.014\ M_{\odot}pc^{-3}$.

Taking into account these contradictory results, we have performed a new analysis (unpublished) based on the Lindblad-Parenago approach. In cylindrical coordinates, the Jeans equation along the z-axis is

$$\frac{1}{\nu_*}\frac{\partial\left(\nu_*\sigma_z^2\right)}{\partial z} + \frac{\partial \Psi}{\partial z} = 0 \qquad \text{II.5.1}$$

where ν_* is the density of the considered stellar (probe) population and Ψ is the total gravitational potential, including contributions both from baryons and dark matter. The corresponding Poisson equation is

$$\frac{\partial^2 \Psi}{\partial r^2} + \frac{1}{r}\frac{\partial \Psi}{\partial r} + \frac{\partial^2 \Psi}{\partial z^2} = 4\pi G \rho_{tot} \qquad \text{II.5.2}$$

where ρ_{tot} is the total matter density (baryons + dark matter). Introduce now the (local) Oort's galactic rotation constants *A* and *B* as

$$A = \frac{1}{4\omega}\left(\frac{\partial^2 \Psi}{\partial r^2} - \frac{1}{r}\frac{\partial \Psi}{\partial r}\right) \; and \; B = \frac{1}{4\omega}\left(\frac{\partial^2 \Psi}{\partial r^2} + \frac{3}{r}\frac{\partial \Psi}{\partial r}\right) \qquad \text{II.5.3}$$

where $\omega = A - B$. Combine eqs. II.5.1, II.5.2 and II.5.3 to obtain, after some algebra

$$4\pi G \rho_{tot} = 2\left(A^2 - B^2\right) - \frac{\partial}{\partial z}\left[\frac{1}{\nu_*}\frac{\partial\left(\nu_*\sigma_z^2\right)}{\partial z}\right] \qquad \text{II.5.4}$$

This equation allows an estimate of the total density in the galactic plane at the solar position from the knowledge of the Oort's constants, the stellar density and the velocity dispersion profiles along the z-axis. Using the Oort's constants derived from Hipparcos data ($A = 14.8 \pm 0.8\ km/s/Kpc$ and $B = -12.4 \pm 0.6\ km/s/Kpc$) and kinematical data from K-dwarves from Kuijken & Gilmore (MNRAS 239, 605, 1989; MNRAS 239, 651, 1989) one obtains for the total matter density $\rho_{tot} = 0.113 \pm 0.023$ M⊙pc^{-3} and a dark matter density $\rho_{dm} = 0.018 \pm 0.010$ M⊙pc^{-3} (or 0.69 GeVcm^{-3}). These values are consistent with Garbari et al. but indicate a dark matter density in the solar neighborhood twice the value usually assumed.

Globular clusters (GC) can also be used as probes of the gravitational potential of the halo, since they are distributed almost spherically around the galactic center up to distances of 30 Kpc. Following the analysis by Borges & de Freitas Pacheco (Ap&SS 153, 67, 1989), F-clusters were distributed in bins corresponding to the following distance intervals: 0-5 Kpc, 5-11 Kpc and 11-20 Kpc. Then, the velocity dispersion was computed for each bin and the results are shown in fig. 6. Notice that at least for distances of the order of 20 Kpc a "heating" of the system is observed, a fact also remarked by other authors. Anyway, it would be temerarious to extrapolate such a trend to higher distances since a decrease (or "cooling") of the velocity dispersion must occur at the outskirts of the halo.

Figure 6
Velocity dispersion profile for galactic globular clusters

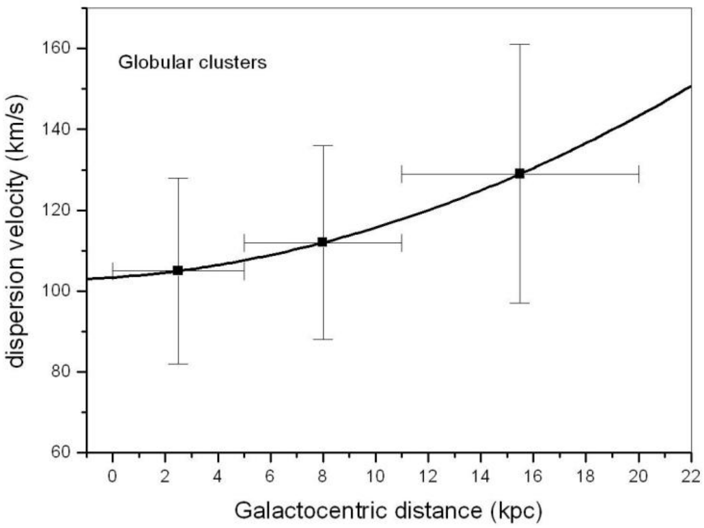

On the other hand, the density of GC decreases from the center of the Galaxy according to $n_{gc} \propto r^{-10/3}$. If GC trace the halo potential, the Jeans equation can be used to compute the total mass inside the radius *r*, i.e.,

$$M_h(\leq r) = -\frac{r^2}{Gn_{gc}} \frac{\partial\left(n_{gc}\sigma_r^2\right)}{\partial r} \qquad \text{II.5.5}$$

Then, the dark matter density can be estimated from the trivial relation

$$\rho_{dm}(r) = \frac{1}{4\pi r^2} \frac{dM_h(r)}{dr} \qquad \text{II.5.6}$$

The numerical solution of these equations permits to compute the dark matter density at r = 8.5 Kpc, distance of the Sun to the galactic centre. The derived density is $\rho_{dm} = 0.011$ $M_{\odot}pc^{-3}$, consistent with the value obtained from the analysis of K-dwarves.

II.6 Dark Matter at Cosmological Scales

Different methods permit to estimate the amount of dark matter at cosmological scales. At such large scales, one measures generally the density parameter Ω_{dm} that is the present ratio between the dark matter density to the critical density, i.e., $\Omega_{dm} = 8\pi G\rho_{dm} / 3H_0^2$.

A relation between the random motion of galaxies not belonging to rich groups or clusters and the density parameter is given by the "cosmic virial theorem" by Peebles (The Large-Scale Structure of the Universe – Princeton Press – 1980), given by

$$\left\langle \sigma_{3D}^2 \right\rangle < \frac{4}{n+7} H_0^2 \Omega_m J_2 \qquad \text{II.6.1}$$

where $\left\langle \sigma_{3D}^2 \right\rangle$ is the square average of the velocity dispersion (random or peculiar motion) of galaxies, n is the exponent of the primordial power spectrum of the density fluctuations and J_2 is the second moment of the galaxy-galaxy correlation function. Bruno & de Freitas Pacheco (ASP 24, 173, 1992) considered a sample of 301 E-galaxies and using a two-parameter distance indicator (effective radius and central stellar velocity of the galaxy), after correcting for the bulk motion due to the Great Attractor, they found for the mean random motion of galaxies $\sigma_{3D} = 352 Km/s$. Using the value of J_2 derived from the CfA redshift survey, i.e., $J_2 = 150h^{-2}Mpc^2$, they obtained that $\Omega_m > 0.16$. Notice that this value is already 4 times higher than the limits imposed by the primordial nucleosynthesis.

The analysis of the galaxy-galaxy auto-correlation function provides also information on the density parameter, since it appear implicitly in the transfer function. The galaxy-galaxy auto-correlation function in the linear theory is related to the inverse Fourier transform of the power spectrum of the primordial density fluctuations, Thus, by measuring the auto-correlation function of galaxies, the power spectrum of the fluctuations can be accessed and by a fitting procedure (see Cole et al., MNRAS 362, 505, 2005) one obtains: $\Omega_m = 0.27$ and $\Omega_b / \Omega_m = 0.18$, in excellent agreement with seven years WMAP data.

The density parameter can be also estimated from the motion of the Local Group of galaxies towards the Virgo cluster (Silk, ApJ 193, 525, 1974). Originally, such a flow was detected in the CfA redshift survey with a velocity of about 470 km/s (Tonry & Davis, ApJ 246, 680, 1981). Further analyses indicated lower velocities, of the order of 200 km/s (Dressler, ApJ 281, 512, 1984; de Freitas Pacheco, AJ 90, 1007, 1985; Tamman & Sandage, ApJ 294, 81, 1985; Federspiel et al., ApJ 495, 115, 1998; Peirani & de Freitas Pacheco, New Astron. 11, 325, 2006). Using the linear theory (see details in Section III.1), the expected velocity of the flow is

$$V_p = \frac{1}{3} H_0 D < \delta > f(\Omega_m) \qquad \text{II.6.2}$$

Taking $H_0 D = 1180\,Km/s$ as the Hubble flow velocity at the Virgo center, $<\delta>=1.72$ the average density inside a sphere of radius D and $V_p = 200\,Km/s$, it results from II.6.2 that the expected growth factor is $f(\Omega_m) = 0.295$ and, consequently, $\Omega_m = 0.12$ (corrections to the linear theory give a higher value, more compatible with the actual data), which indicates a value 4 times that resulting from the primordial nucleosynthesis.

Dark matter structures (filaments and halos of the cosmic web) are responsible for weak lensing of distance sources (see Massey et al. Rep.Prog.Phys. 73, 086901, 2010). The analysis of the distortion of the shape of galaxies ("shear") by weak lensing permits an estimate of the mean global matter density. Lesgourgues et al. (arXiv:0705.0533) obtained by such a procedure $\Omega_m = 0.247 \pm 0.016$, in good agreement with WMAP data.

III. The Decoupling of Dark Matter

Dark matter particles decouple very early in the history of the universe from the cosmic plasma. The decoupling occurs when the interaction timescale between dark matter particles becomes equal to the expansion timescale. At this characteristic time t_* if the mass of the DM particle, in comparison with the plasma temperature, satisfies the condition $m_\chi c^2 > kT$, then particles decouple when they are non-relativistic. In the opposite sense, the decoupling occurs when particles are relativistic. It is generally accepted that DM particles are massive enough to decouple non-relativistically in order to be very "cold" when the formation of structures begins thanks to the gravitational instability. Primordial DM density fluctuations after decoupling are able to grow and to have the required amplitude observed in temperature maps of the CMB.

When thermal equilibrium disappears, particles begin to annihilate until their abundance becomes "frozen" because the expansion rate is faster than the annihilation rate. The annihilation process of particles X is governed by the equation

$$\frac{dn_X}{dt} + 3Hn_X = -n_X \bar{n}_X < \sigma_X v > + P_X \qquad \text{III.1}$$

In this equation n_X and $\bar{n}_X$ are respectively the density of particles and anti-particles of species X, the first term on the right represents the annihilation rate and the last, the production rate. Clearly, in thermal equilibrium both terms on the right side of the above equation compensates each other. In this case, denoting n_{eq} the density at thermal equilibrium, equation III.1 can be recast as

$$\frac{dn_X}{dt} + 3Hn_X = -< \sigma_X v > \left(n_X^2 - n_{eq}^2\right) \qquad \text{III.2}$$

where we have assumed an equal density of particles and anti-particles. Define the concentration of species X with respect to photons as $X = n_X / n_\gamma$. Since the comoving photon density is conserved, we get for the evolution of the concentration

$$\frac{dX}{dt} = -<\sigma_X v> n_\gamma \left(X^2 - X_{eq}^2\right) \qquad \text{III.3}$$

Consider now a small deviation from equilibrium such as $X = X_{eq} + \Delta X_{eq}$. Plug this into eq. III.3 to obtain

$$\frac{1}{\Delta X_{eq}} \frac{d\Delta X_{eq}}{dt} = -2 <\sigma_X v> n_\gamma X_{eq} \qquad \text{III.4}$$

The above equation permits to define the "freezing" timescale $t_{fre} = \left|\Delta X_{eq} /(d\Delta X_{eq} / dt)\right|$ since the equilibrium is destroyed when $t_{fre} \geq H^{-1}$. The equality permits to fix the "freezing" time and to estimate the thermal average annihilation cross section. Considering the Hubble equation for a radiation dominated universe, which is valid when DM particles decouple, the thermal average annihilation cross section can be expressed as

$$<\sigma_X v> = \frac{4\pi^3}{\sqrt{90}} \left(\frac{\hbar G^{1/3}}{c}\right)^{3/2} \frac{\sqrt{g_{eff}(T_{fre})}}{m_X g_X} \left(\frac{kT_{fre}}{m_X c^2}\right)^{1/2} \exp\left(\frac{m_X c^2}{kT_{fre}}\right) \qquad \text{III.5}$$

In this equation, symbols have their usual meaning, $g_{eff}(T_{fre)}$ is the number of degrees of freedom of particles present in the cosmic plasma at the freezing point, when the temperature is T_{fre} and g_X is the degree of freedom of particle *X*. Notice that $<\sigma_X v> \propto T^q$, with $q = 0$ for a s-wave and $q = 1$ for a p-wave.

On the other hand, the expected present density parameter Ω_X related to particles *X* can be derived from the knowledge of the concentration of *X* at the freezing point (which remains constant during the remaining evolution of the universe) and the present photon density, i.e.,

$$\Omega_X = \frac{8\pi G}{3H_0^2} \left[\frac{g_{eff}(T_0)}{g_{eff}(T_{fre})}\right] m_X n_{\gamma,0} X_{eq}(T_{fre}) \qquad \text{III.6}$$

where the ratio between degrees of freedom at the freezing point and the present time corrects for the different "heating" episodes associated to annihilation of species. Since from WMAP data $\Omega_{dm} h^2 = 0.1108$, from equation III.6 one obtains for the freezing temperature as a function of the particle mass (given in GeV)

$$T_{fre} \approx 0.048 m_X^{0.9583} GeV \qquad \text{III.7}$$

Using this result and eq. III.5, the thermal average annihilation cross section (in units of 10^{-26} $cm^3 s^{-1}$) can be expressed also as a function of the particle mass (in GeV) as

$$<\sigma_X v> = 0.9447 + 0.11318 \log m_X \qquad \text{III.8}$$

The result above corresponds only to the s-wave contribution. The p-wave contribution amounts to about $4.6\times10^{-28}\,cm^3s^{-1}$ if the particle mass is in the range 30-900 GeV. If one assumes a DM particle of mass equal to 144 GeV, required to explain the putative 130 GeV γ-ray line the total annihilation rate is $1.25\times10^{-26}\,cm^3s^{-1}$ while the value necessary to explain the intensity of the γ-ray line is $2.3\times10^{-27}\,cm^3s^{-1}$. This would suggest that only one fifth of the annihilations goes to the channel $\chi\bar{\chi}\rightarrow Z^0\gamma$ and the remaining goes to the channels $\chi\bar{\chi}\rightarrow W^+W^-, b\bar{b}, \mu^+\mu^-, \tau^+\tau^-$.

III.1 Evolution after Decoupling

After decoupling and "freezing", dark matter particles evolve as a "collisionless" fluid and obey the Vlasov equation. For pedagogical purposes, a non-relativistic treatment will be considered but the basic conclusions are valid in a fully relativistic analysis. The one-particle distribution function $f(\vec{r},\vec{v},t)$ that gives the probability for a given particle in a given instant of time have a velocity $\vec{v}$ at the position $\vec{r}$, satisfies the equation

$$\frac{\partial f}{\partial t}+\vec{v}\cdot\frac{\partial f}{\partial \vec{r}}-\frac{\partial \phi}{\partial \vec{r}}\cdot\frac{\partial f}{\partial \vec{v}}=0 \qquad \text{III.1.1}$$

This equation is coupled to the Poisson equation as

$$\nabla^2\phi=4\pi G\rho=4\pi G\int f(\vec{r},\vec{v},t)d^3v \qquad \text{III.1.2}$$

At the early phases of the matter dominated era, the universe behaves as the Einstein-de Sitter cosmology. Thus, the matter density decreases as the square of the age of the universe, namely

$$\rho=\frac{1}{6\pi G t^2} \qquad \text{III.1.3}$$

Combining this relation with the solution of the Poisson equation, one obtains for the gradient of the gravitational potential

$$\frac{\partial \phi}{\partial r}=\frac{4\pi G}{3}\rho r=\frac{2}{9}\frac{r}{t^2} \qquad \text{III.1.4}$$

On the other hand, the characteristics of the Vlasov equation III.1.1 are

$$dt=\frac{dx_i}{v_i}=-\frac{dv_i}{(2x_i/9t^2)} \qquad \text{III.1.5}$$

A solution of this system of equations is

$$I=v_it^{2/3}-\frac{2}{3}x_it^{-1/3} \qquad \text{III.1.6}$$

Recalling that the scale factor in the Einstein-de Sitter model varies as $a \propto t^{2/3}$, the equation above can be recast as

$$u_i = a(v_i - Hx_i) \qquad \text{III.1.7}$$

Since solutions of the Vlasov equation can be expressed in terms of the characteristics, let us assume

$$f = A\exp\left[-\frac{a^2}{\theta^2}\left(\vec{v} - H\vec{r}\right)^2\right] \qquad \text{III.1.8}$$

where A is a normalization constant that can be estimated from the condition that the integral in velocity space should be equal to the matter density (see eq. III.1.2). Thus,

$$f(\vec{r},\vec{v},t) = \frac{1}{6\pi^{5/2}G\theta^3 t_0^2}\exp\left[-\frac{a^2}{\theta^2}\left(\vec{v} - H\vec{r}\right)^2\right] \qquad \text{III.1.9}$$

where t_0 is the present age of the universe and, without loss of generality we have put $\vec{r} = 0$.

Let us evaluate the mean square velocity using the distribution function III.1.9. A simple calculation gives

$$< v^2 >= \frac{3\theta^2}{2a^2} \qquad \text{III.1.10}$$

The above relation expresses a well known result: the kinetic energy of the particle decreases as square of the scale factor during the expansion of the universe. Define now the quantity $Q_{1D} = \rho / < v_z^2 >^{3/2}$, which is an indicator of the phase space density. Using eq. III.1.10 and supposing isotropic motion, one obtains

$$Q_{1D} = \sqrt{8}\,\frac{\rho a^3}{\theta^3} \qquad \text{III.1.11}$$

Since in the Einstein-de Sitter model $\rho a^3 =$ constant, the phase space density indicator is also constant. Thus, collisionless particles evolve satisfying the constancy of the phase space density, which will be violated only when structures begin to be formed. It is useful to estimate the value of Q_{1D} at the freezing point. The 1D velocity dispersion is $\sigma_{1D}^2 = Y_{fre}^{-1}c$ and the density is

$$\rho_x(T_{fre}) = \frac{g_x m_x^4}{\sqrt{8}}\left(\frac{c}{\hbar}\right)^3 Y_{fre}^{-3/2} e^{-Y_{fre}} \qquad \text{III.1.12}$$

where we have introduced $Y_{fre} = m_x c^2 / kT_{fre}$. Thus, the initial phase space density indicator of dark matter particles is

$$Q_{1D} = \frac{g_x}{\sqrt{8}} \frac{m_x^4}{\hbar^3} e^{-Y_{fre}} \qquad \text{III.1.13}$$

As a consequence, if the value of Q_{1D} could be estimated from observations, the mass of the dark matter particle could be estimated. Unfortunately, as we shall see later, when structures begin to be formed, dark matter relaxes trough “violent relaxation”, a process that reduces by several orders of magnitude the available phase space density.

III.2. The Growth of Linear Perturbations

Primordial fluctuations originated probably during the inflation era, are able to grow once dark matter particles decouple from the highly relativistic plasma. In fact, the amplitude of these fluctuations is seen is in the temperature map of the CMB, being of the order of $\Delta\rho/\rho \approx 10^{-4}$. A natural question rises: for baryons, the minimal gravitational unstable scale corresponds to the Jeans length. What is the corresponding scale for dark matter? Starting with the Vlasov equation (see eq. III.1.1), we first integrate all terms in the velocity space. The resulting equation is

$$\frac{\partial\rho}{\partial t} + \frac{\partial\rho < v_i >}{\partial x_i} = 0 \qquad \text{III.2.1}$$

that simply expresses the mass conservation. Then, multiply the Vlasov equation by the velocity component v_j and integrate again over velocities to obtain the momentum conservation equation

$$\frac{\partial\rho < v_j >}{\partial t} + \frac{\partial\rho < v_i v_j >}{\partial x_i} + \rho\frac{\partial\phi}{\partial x_j} = 0 \qquad \text{III.2.2}$$

In the next step, multiply eq. III.2.1 (mass conservation) by the velocity component v_j and subtract from eq. III.2.2

$$\rho\frac{\partial < v_j >}{\partial t} - < v_j > \frac{\partial\rho < v_j >}{\partial x_j} + \frac{\partial\rho < v_i v_j >}{\partial x_i} + \rho\frac{\partial\phi}{\partial x_j} = 0 \qquad \text{III.2.3}$$

Introduce now the velocity dispersion tensor

$$\sigma_{ij}^2 = \left\langle \left(v_i - < v_i >\right)\left(v_j - < v_j >\right) \right\rangle = < v_i v_j > - < v_i >< v_j > \qquad \text{III.2.4}$$

Substitute III.2.4 into III.2.3 to obtain finally for the momentum conservation equation

$$\frac{\partial < v_j >}{\partial t} + < v_j > \frac{\partial < v_j >}{\partial x_j} + \frac{1}{\rho}\frac{\partial\rho\sigma_{ij}^2}{\partial x_i} + \frac{\partial\phi}{\partial x_j} = 0 \qquad \text{III.2.5}$$

Once the main conservation equations were derived, the following assumptions are made to get the linear approximation: a) the flow velocity is a combination of the Hubble flow and peculiar velocities, i.e., $<\vec{v}>=\vec{V}_H+\vec{V}_p$; b) peculiar velocities are small in comparison with the Hubble flow, in particular in the early universe; c) the velocity dispersion of peculiar motions is isotropic, i.e., $\sigma_{ij}^2=\sigma^2\delta_{ij}$; d) the density contrast $\delta(\vec{r},t)=\left[\rho_1(\vec{r},t)-\rho_b(t)\right]/\rho_b(t)$, where $\rho_b(t)$ is the matter density of the expanding background satisfies the condition $\delta(\vec{r},t)<<1$; e) in absence of strong relaxation processes, the evolution of density fluctuations occurs keeping constant the phase space density indicator Q_{1D}, which hereafter will be denoted simply by Q. This hypothesis is equivalent to say that the variations in density are adiabatic, since the entropy density is related to the phase-space density by $S\propto-\lg Q$. Under these conditions, the effective pressure term $\rho\sigma^2$, appearing in III.2.5, leads to a perturbed effective pressure $P_1(r,t)=\frac{5}{3}\frac{\rho_b^{5/3}(t)}{Q^{2/3}}\delta(r,t)$. Thus, the linearization of the mass conservation equation, Poisson equation and momentum conservation equation leads to the system:

$$\frac{\partial\delta}{\partial t}+\vec{\nabla}\cdot\vec{V}_p=0 \qquad \text{III.2.6}$$

$$\nabla^2\phi=4\pi G\rho_b\delta \qquad \text{III.2.7}$$

and

$$\frac{\partial\vec{V}_p}{\partial t}+H\vec{V}_p+\frac{5}{3}\left(\frac{\rho_b}{Q}\right)^{2/3}\vec{\nabla}\delta+\vec{\nabla}\phi=0 \qquad \text{III.2.8}$$

where, as usually, the Hubble parameter is related to the scale factor a by $H=d\lg a/dt$. Introduce now comoving coordinates $\vec{x}$ related to physical coordinates by $\vec{r}=a\vec{x}$ and take the Fourier transform (defined in the comoving frame) of the perturbed quantities. Under these conditions, the Fourier components of the linearized equations are

$$\frac{\partial\delta_k}{\partial t}+\frac{i\vec{k}\cdot\vec{V}_k}{a}=0 \qquad \text{III.2.9}$$

$$-\frac{k^2}{a^2}\phi_k=4\pi G\rho_b\delta_k \qquad \text{III.2.10}$$

and

$$\frac{\partial\vec{V}_k}{\partial t}+H\vec{V}_k+\frac{5}{3}\left(\frac{\rho_b}{Q}\right)^{2/3}\frac{i\vec{k}}{a}\delta_k+\frac{i\vec{k}}{a}\phi_k=0 \qquad \text{III.2.11}$$

After some algebraic manipulation, we get for the evolution of the density contrast

$$\frac{\partial^2 \delta_k}{\partial t^2} + 2H\frac{\partial \delta_k}{\partial t} + \left[\frac{5}{3}\left(\frac{\rho_b}{Q}\right)^{2/3}\frac{k^2}{a^2} - 4\pi G\rho_b\right]\delta_k = 0 \qquad \text{III.2.12}$$

Gravitational instability requires that the bracketed term in III.2.12 be negative, which implies the existence of a minimum wavelength λ_J above which perturbations grow and given by

$$a^2\lambda_J^2 = \frac{5\pi}{3GQ^{2/3}\rho_b^{1/3}} \qquad \text{III.2.13}$$

Notice that for dark matter the critical length (or Jeans length) depends inversely on the phase space density or, equivalently, on the mass of the dark matter particle. As in the baryonic case, a critical mass (or the Jeans mass) can be defined by

$$M_J = \frac{\pi}{6}\rho_b\lambda_J^3 = \sqrt{\frac{125}{972}}\pi^{5/2}\rho_b^{1/2}G^{-3/2}Q^{-1} \qquad \text{III.2.14}$$

The equation above can be expressed in terms of the redshift as

$$M_J = 7.91\times 10^{-37}\sqrt{\Omega_{dm}h^2}(1+z)^{3/2}Q^{-1}\ \ M_\odot \qquad \text{III.2.15}$$

It worth mentioning that the Jeans mass for dark matter increases with the redshift, an opposite behavior of baryonic matter whose Jeans mass decreases with the redshift. If the mass of the DM particle is fixed, then the freezing temperature can be estimated (see eq. III.7) as well as the corresponding redshift and the phase space density indicator (eq. III.1.13). These quantities permit an evaluation of the Jeans mass from III.2.15. For DM particles having masses in the range 100-200 GeV, the Jeans mass varies from 2.88 x 10^4 $M_\odot$ down to 1.02 x 10^4 $M_\odot$. These values represent probably the lowest possible masses for dark matter halos.

III.3 Warm Dark Matter

Particles decoupling relativistically may have presently, depending on their masses, a non-negligible velocity dispersion. However, as mentioned previously, these particles stream freely up to the matter-radiation equality, defining a scale λ_f below which perturbations are erased. The comoving free streaming scale is given by

$$\lambda_f \approx 3.15\frac{kT_0}{m_x cA}\left[1 + \lg\left(\frac{1+z_{NR}}{1+z_{eq}}\right)\right] \qquad \text{III.3.1}$$

In this equation T_0 is the present CMB temperature, m_x is the particle mass, z_{NR} is the redshift at which the particle becomes non-relativistic and z_{eq} is the redshift at matter-radiation equality. The parameter A is defined by

$$A^2 = \frac{8\pi G}{3c^2} g_{eff}(T_{fre}) u_{\gamma,0} \qquad \text{III.3.2}$$

including, besides usual constants, the effective number of degrees of freedom at the freezing point $g_{eff}(T_{fre})$ and the present energy density of CMB photons $u_{\gamma,0}$. Numerically, the free streaming scale can be written as

$$\lambda_f \approx \frac{0.46}{m_{keV}\sqrt{g_{eff}(T_{fre})}} \left[1 + \lg(407 m_{keV})\right] \; Mpc \qquad \text{III.3.3}$$

If the WDM particle mass is conveniently chosen, the free streaming acts as a filter, erasing masses below the characteristic scale

$$M_f = \frac{4\pi}{3} \rho_b \lambda_f^3 \approx 1.12\times 10^{12} \Omega_m h^2 \lambda_f^3 \; M_\odot \qquad \text{III.3.4}$$

where λ_f is in *Mpc*. Moreover, simulations suggest that even cored dark matter profiles can be obtained (Maccio et al., arXiv:1202.1282). A generally invoked candidate is the sterile neutrino, whose mass is expected to be around 2 keV. In this case, the free streaming scale is about 0.54 Mpc and the characteristic mass scale is about $2\text{x}10^{10}$ $M_\odot$. However, for these values, the simulations by Maccio et al. indicate that the core radius is too small, namely, of de order of 10 pc only. If one requires for such a mass scale a core radius of about 1.0 Kpc, i.e., two orders of magnitude larger, then the mass of the putative sterile neutrino should be around 0.1 keV. Particles with such a mass have a free streaming scale of about 6.6 Mpc and a characteristic mass scale of $4.3\text{x}10^{13}$ $M_\odot$ and, in this case, besides dwarf galaxies even bright and massive objects are erased.

IV. Relaxation of Collisionless Systems

Dark matter particles interact only through gravitation and, if halos are in dynamical equilibrium (or in “quasi”-equilibrium), it is important to understand the mechanisms leading to such a relaxed state. Elliptical galaxies are old stellar systems, which can be imagined to be constituted by a collisionless (stellar) fluid. The nearly “universal” brightness profiles seen in these objects require short timescale processes and no dependence on the stellar mass, otherwise significant color gradients would be observed (see, for instance, de Freitas Pacheco et al., Recent Research Developments in Astronomy & Astrophysics, 1, 271, 2003). Concerning dark halos, cosmological simulations indicate that these structures have peaked density profiles (Navarro et al. MNRAS 275, 56, 1995 and ApJ 62, 563, 1996). If density fluctuations have an initial power spectrum of the form $P(k) \propto k^n$ in an Einstein-de Sitter universe, then halos are expected to have a density profile $\rho \propto r^{-(9+3n)/(4+n)}$ (Hoffman & Shaham, ApJ 297, 16, 1985) and the behavior of the Navarro-Frenk-White (NFW) profile in the central region of halos is recovered only for n >> 1.

A short relaxation timescale cannot be obtained via two-body interactions since the expected timescale in longer than the Hubble time. Relaxation processes in the presence of a variable gravitational potential has been investigated since the sixties by Michel Hénon (Hénon, Ann.Astrophys. 27, 83, 1964). His simulations indicate that the system reach equilibrium in a timescale of the order of the dynamical timescale, i.e., $t \propto 1/\sqrt{G\rho_0}$ where ρ_0 is the initial mean density of the system. After the numerical experiments by Hénon, the concept of "violent" relaxation (VR) was developed by Lynden-Bell (MNRAS 136, 101, 1967). VR describes how a collisionless system relaxes from an initial chaotic state to quasi-equilibrium, when rapid changes in the gravitational potential occur during the gravitational collapse or following a merger episode. A fundamental characteristic of the Lynden-Bell theory is that the resulting particle energy distribution is "Fermi-like". These ideas were revisited by Shu (ApJ 225, 83, 1978), who concluded that collisionless relaxation via chaotic changes of the collective gravitational potential lead to no mass segregation and that stars of different masses have the **same velocity dispersion** (not the same temperature). In realistic collisionless systems the velocity distribution is probably Maxwellian and, according to the conclusions by Nakamura (ApJ 531, 739, 2000), collective effects like phase-mixing produce a Gaussian velocity distribution independent on the particle mass. Gaussian velocity distributions were found in N-body simulations by Merrall & Henriksen (arXiv:0306268) and by Diemand et al. (MNRAS 352, 535, 2004). The latter authors also found that the velocity distribution has a negative kurtosis, meaning a distribution with a flat topped profile.

The difficulty to describe these fully non-linear processes leading to the (quasi) equilibrium state of collisionless systems demands the use of numerical tools. A panoply of simulations on the subject has been reported in the literature in the past years. Here, we will be concerned only to some specific results.

The first point concerns the central slope $d\lg\rho/d\lg r$ of the density profile of halos. According to Klypin et al. (ApJ 554, 903, 2001), such a slope may depend on the merger history while Ascasibar et al. (MNRAS 352, 1109, 2004) suggest a dependence on the initial conditions.

The second aspect concerns the phase density indicator *Q*. High resolution simulations indicate that $Q \propto r^{-\beta}$, where the exponent $\beta \approx 1.87$ is the same either for galaxy-size halos (Taylor & Navarro, ApJ 563, 483, 2001) or cluster-size halos (Rasia et al., MNRAS 351, 237, 2004). Such a power-law profile for the phase space density could be a consequence of the hierarchical assembly of halos that preserves stratification or to be a generic feature of the violent relaxation process (Williams et al., arXiv:0412442).

IV.1 A Toy Model for Halos

In this section a self-consistent toy model for dark matter halos will be examined. This model reproduces quite well the density profile resulting from simulations, excepting for the very central regions and reproduces the power low profile observed for the phase space density indicator *Q*. Moreover, the velocity distribution has a negative kurtosis, i.e., the velocity distribution has a flat topped profile as seen in most simulations.

We assume that the halo is characterized by a power law distribution for the energy of dark matter particles, i.e.,

$$f(E) = K\left|E\right|^{p} \qquad \text{IV.1.1}$$

where K is a normalization constant and $E = V^2/2 - \phi(r)$. Since gravitationally bound particles must have negative energies, the maximum velocity at a distance r from the halo center is $V_{\max}^2 = 2\phi(r)$, corresponding to a particle of zero energy. The density can be derived from

$$\rho(r) = \int_0^{V_{\max}} f(E) d^3V = \frac{4\pi\sqrt{2}\, K\, \Gamma(3/2)\Gamma(p+1)}{\Gamma(p+5/2)} \phi^{p+3/2} \qquad \text{IV.1.2}$$

In other to compute the integral, we have used IV.1.1 and the definition of the energy. Similarly, the velocity dispersion of DM particles at the distance r from the halo center can be calculated as

$$\rho(r)\sigma^2 = \int_0^{V_{\max}} V^2 f(E) d^3V = \frac{8\pi\sqrt{2}\, K\, \Gamma(5/2)\Gamma(p+1)}{\Gamma(p+7/2)} \phi^{p+5/2} \qquad \text{IV.1.3}$$

Assume that the system is in equilibrium, has spherical symmetry and an isotropic velocity distribution. Under these conditions, the system is described by the following Jeans equation

$$\frac{1}{3}\frac{\partial \rho\sigma^2}{\partial r} + \rho \frac{GM(r)}{r^2} = 0 \qquad \text{IV.1.4}$$

which can be rewritten as

$$\frac{r^2}{3\rho}\frac{\partial \rho\sigma^2}{\partial r} = -GM(r) \qquad \text{IV.1.5}$$

Then, differentiate both sides of the above equation with respect to the radial coordinate

$$\frac{\partial}{\partial r}\left[\frac{r^2}{3\rho}\frac{\partial \rho\sigma^2}{\partial r}\right] = -G\frac{\partial M(r)}{\partial r} = -4\pi G\rho r^2 \qquad \text{IV.1.6}$$

Replace eqs. IV.1.2 and IV.1.3 into the equation above to obtain finally

$$\frac{1}{r^2}\frac{\partial}{\partial r}\left[r^2 \frac{\partial \phi}{\partial r}\right] + A\phi^{p+3/2} = 0 \qquad \text{IV.1.7}$$

where A is a constant including all previous constants. The equation above is a Lane-Emden equation for the gravitational potential and describes a system with a polytropic equation of state. Despite the existence of non-singular solutions for the Lane-Emden equation, which do not describe adequately the structure of halos, we consider singular solutions of the form $\phi \propto r^{-\beta}$. These solutions exist if p > 3/2 and β = 4/(2p+1). As we shall see, halos can be reasonably described by the particular case p = 9/2 or β = 2/5. Then, the density profile varies as $\rho \propto \phi^{p+3/2} \propto r^{-12/5}$ and the phase density indicator varies as $Q \propto \phi^{p} \propto r^{-9/5}$. Figures 7 and 8 compare these theoretical expectations with simulated data by Taylor & Navarro (ApJ 563, 483, 2001).

Figure 7
Predicted (solid line) and simulated density profile of a dark matter halo. Data indicate a steeper slope only in the very central regions.

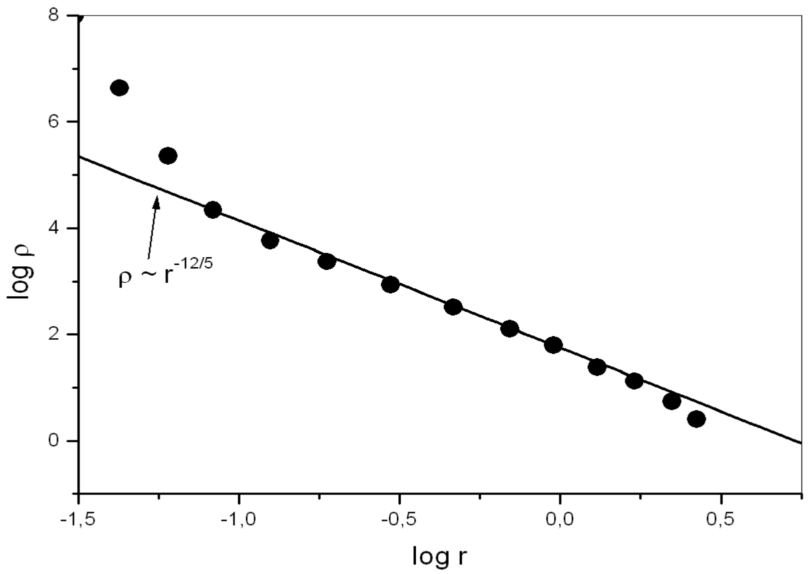

Figure 8
Predicted (solid line) and simulated phase-space density indicator Q.

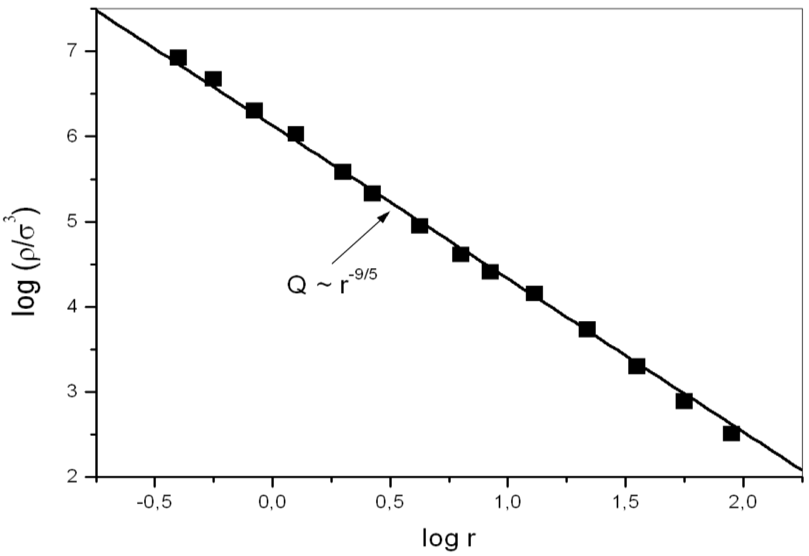

The velocity distribution can be computed from the relation

$$\frac{dF(V)}{dV} = BV^2\left(V_{\max}^2(r) - V^2\right)^{9/2} \qquad \text{IV.1.8}$$

where B is a normalization constant and the maximum velocity $V_{\max}$ was defined previously. If we consider a spherical shell in which the maximum velocity is 300 km/s, one obtains for the velocity dispersion a value of 139 km/s. On the other hand, the normalized kurtosis of the considered velocity distribution is $\kappa = (\mu_4 / \mu_2^2) - 3$ = - 1.54. This negative kurtosis indicates a flat-topped distribution as observed in simulations. Figure 9 shows data points derived from the velocity distribution IV.1.8 with $V_{\max}$ =300 km/s (filled squares) and the best fitted Gaussian (red curve). Notice that this Gaussian has a velocity dispersion of only 55 km/s, indicating that the distribution IV.1.8 is in fact broader. In conclusion, this simple self-consistent model explains quite well some basic features of dark matter halos, namely, the external density profile, the power law profile of the phase space density indicator and a flat-topped velocity distribution

Figure 9
Velocity distribution derived from the toy model (filled squares) fitted by a Gaussian

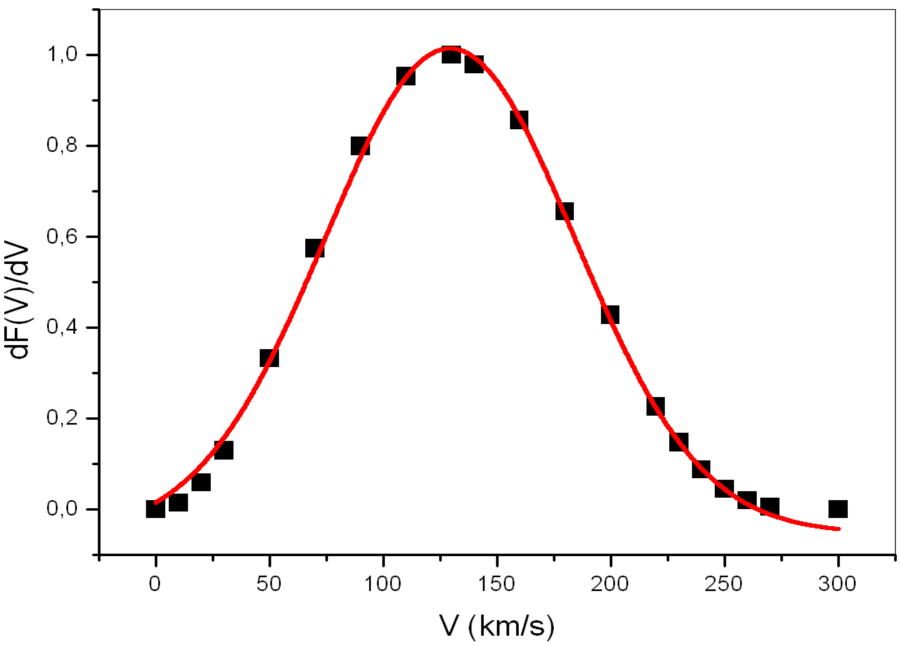

IV.2 Dynamical Evolution of Halos

In the previous section we have examined the equilibrium state of halos. However, halos are in continuous evolution, since they grow either by accreting mass "quietly", via filaments constituting the cosmic web or "violently", via merger episodes. The latter process, as we shall see, reduces the phase space density and, on the average, increases the angular momentum of halos. All processes occurring during a merger event are strongly non-linear and must be studied through numerical simulations.

Here are described the results derived from cosmological simulations including only dark matter (Peirani et al., MNRAS 367, 1011, 2006). These simulations have a mass resolution of 2.05×10^8 $M_\odot$, sampling a volume of the universe of $27000 h^{-3}$ Mpc^3. Halos were followed from z = 50 up to z = 0. Simulations including both "cold" and "warm" dark matter were performed. The latter corresponding to particles with a mass of 0.5 keV that have a free streaming scale of 1.8 Mpc and a mass scale of 8×10^{11} $M_\odot$.

Once that halos have been identified by a percolation algorithm, unbound particles (with positive total energies) are eliminated. Thus, only gravitationally bound structures are retained. Halos were classified into two categories: those that have grown only by accretion and those that have been assembled (besides accretion) by fusions. These events are characterized by the merger of a main halo and another having at least a mass equal to 1/3 of the main object (computations modifying the criterion, i.e., considering a limit of 1/6 do not change substantially the results). The first aspect concerns the growth of halos or, in other words, how their masses evolve. For each redshift the mass distribution of halos is computed as well as the median of the distribution. Two regimes are clearly seen: an initial rapid growth followed by a more slowly gain of mass. The evolution of the median of the distribution is shown in figure 10.

Figure 10
Evolution of the median of the mass distribution of halos

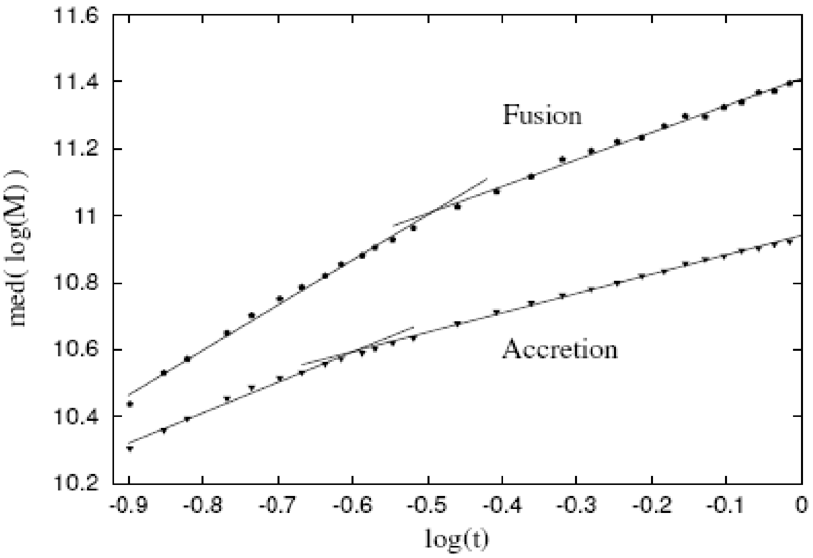

The evolution can be described by power laws of the form $M_{med} \propto t^{\alpha}$. For halos assembled essentially by accretion, $\alpha = 0.91$ for z > 1.8 and $\alpha = 0.58$ for z < 1.8 while for halos having suffered important fusions $\alpha = 1.35$ for z > 1.5 and $\alpha = 0.81$ for z < 1.5. Clearly, the later class of halos grows faster and attains mass values higher than halos of the former category. The existence of two regimes is probably a consequence of the transition observed in the total rate of fusion occurring at z ~ 1.5, which is drastically reduced beyond this moment. It is interesting to mention that in a hierarchical scenario, if the power spectrum of the density fluctuation is of the form $\left|\delta_k^2\right| \propto k^n$ (Peebles, The Large-Scale Structure of the Universe – Princeton Press – 19880) then the mass of the fluctuations grows as $m \propto t^{4/(3+n)}$. Thus, for a Harrison-Zeldovich spectrum, the mass grows linearly with time, close to the results of simulations. Moreover, Toth & Ostriker (ApJ 389, 5, 1992) computed the expected growth for a CDM power spectrum and derived $m \propto t^{1.3}$, in agreement with simulations.

Similarly, the **total** energy of halos scales as a power-law with different exponents according to the redshift and according to the main process of assemblage. The evolution of the median of the (absolute values of the) energy distribution is shown in figure 11. An immediate conclusion is that halos having being assembled by different merger events are more bound than halos that have grown by accretion only.

The median of the energy distribution evolves as $|E| \propto t^{\beta}$, where $\beta = 1.32$ for z > 1.8, $\beta = 0.66$ for z < 1.8 for halos that have grown by accretion and $\beta = 1.93$ for z > 1.5, $\beta = 1.03$ for z < 1.5, for halos assembled by significant merger events.

Another fundamental aspect concerns the dynamical state of halos. It is generally assumed in the literature that once halos collapse they attain equilibrium. The analysis is essentially based on the spherical model or the Press-Schechter approach (see details in the next section). However, even after the collapse, halos continue to grow by accretion or mergers that destroy their equilibrium state. Thus halos are always relaxing or searching for equilibrium. On the average, deviations from equilibrium can be quantified by the virial ratio $r_V = 2T/|W|$, which in equilibrium is equal to one. Higher values indicate "expansion" and lower values indicate "contraction".

Figure 11
Evolution of the median of the total energy distribution of halos

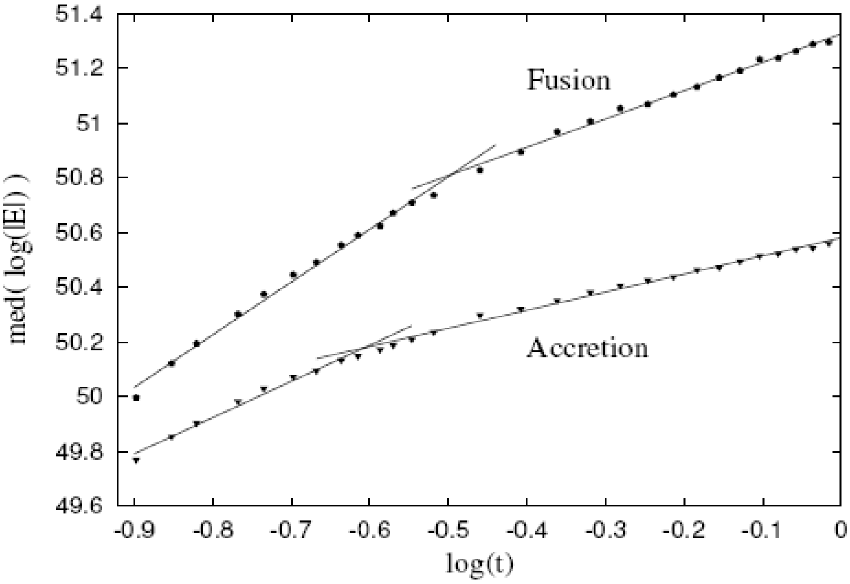

In figure 12 it is shown the evolution of the average value of the virial ratio for CDM and WDM for halos of both classes. Notice that for CDM the average virial ratio decreases as $r_V \propto t^{-0.123}$, reaches the unity at z ~ 0.25 and then becomes slightly smaller. WDM halos, on the average, have not yet reached a fully equilibrium state. When considered separately, CDM halos assembled only by accretion reach $r_V = 1$ at z ~ 0.61 while those assembled by important fusion events have not yet reached equilibrium on the average. This confirms that fusions destroy the equilibrium state reached just after shell crossing (see next section)

Figure 12
Evolution of the average value of the virial ratio

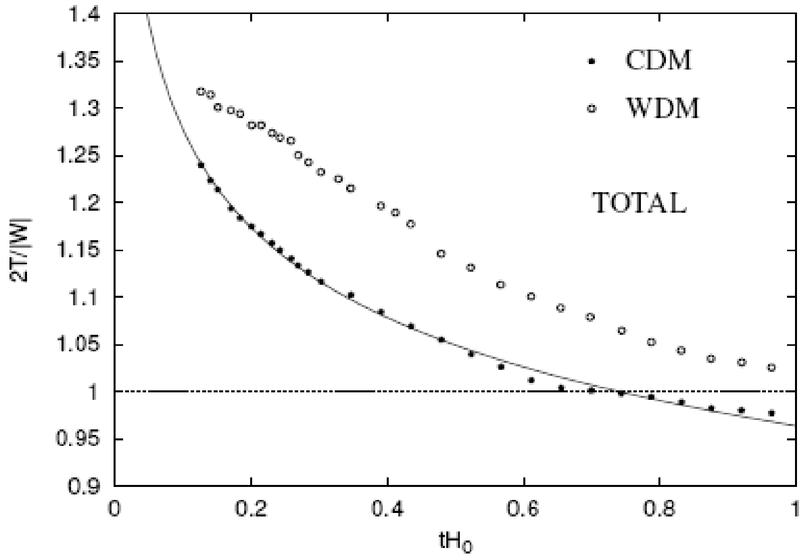

Instead of considering average values, the distribution of the virial ratio as a function of the halo mass can be investigated. This is done in figure 13 where it can be seen that only a small fraction of the halos have $r_V = 1$. In general, low mass halos are still contracting while massive halos have a tendency to "expand".

Figure 13
Distribution of the virial ratio as a function of the halo mass

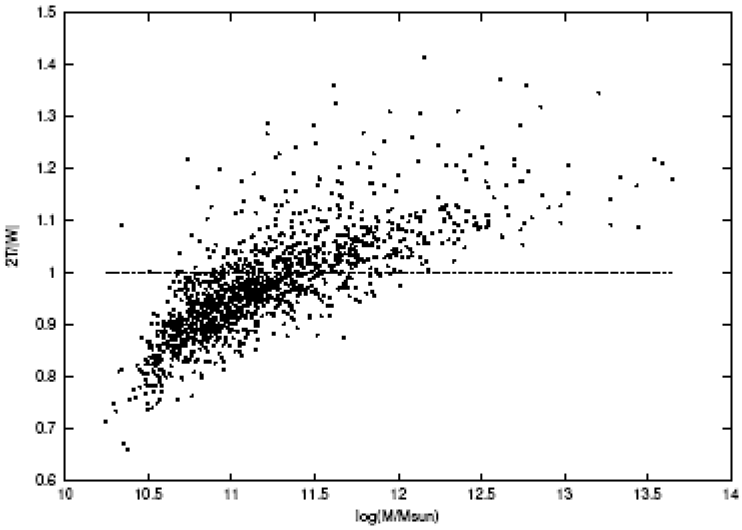

IV.2.1 Evolution of the phase-space density indicator

The early evolution of Q can be understood if the Press-Schechter approach is adopted, namely, a spherical symmetric overdense region evolves as a closed universe. As long as the expansion of the universe is matter dominated, the external radius R enclosing a mass M obeys the equation

$$\frac{d^2R}{dt^2} = -\frac{GM}{R^2} \qquad \text{IV.2.1.1}$$

This equation can be trivially integrated and one obtains

$$\frac{1}{2}\left(\frac{dR}{dt}\right)^2 = \frac{GM}{R} + E \qquad \text{IV.2.1.2}$$

where E is an integration constant. The above equation can be rewritten as

$$\left(\frac{\dot{R}}{R}\right)^2 = \frac{2GM}{R^3} + \frac{2E}{R^2} \Leftrightarrow \left(\frac{\dot{a}}{a}\right)^2 = \frac{8\pi G}{3}\rho - \frac{Kc^2}{a^2} \qquad \text{IV.2.1.3}$$

which can be formally identified with the Hubble equation if we put $M = 4\pi R^3 \rho / 3$ and $2E = -Kc^2$. Then, the integration constant (the total energy) is related to the curvature of a closed world-model. The parametric solution of IV.2.1.2 (or IV.2.1.3) is well known and given by

$$R = \frac{R_{\max}}{2}\left(1 - \cos\theta\right)$$
$$t = \frac{t_{col}}{2\pi}\left(\theta - \sin\theta\right) \qquad \text{IV.2.1.4}$$

The spherical perturbation expands initially as fast as the background, but the density contrast increases, reaches a maximum expansion at $\theta = \pi$ when the kinetic energy is zero, detaches from the expanding background and then contracts until a complete collapse at $\theta = 2\pi$. During the final contracting phase, the potential energy is comparable to the kinetic energy and the rapid variation of the potential transfer energy from bulk motions to random motions (violent relaxation) until equilibrium is reached in a timescale $t_{col} = \pi^2 R_{\max}^3 / 2GM$. This last phase is characterized by the crossing of different infalling shells and is dubbed “shell crossing” phase. Simple algebra shows that the density contrast after collapse is $\rho_V / \rho_b = 18\pi^2 \approx 177.6$. Some observers use the round value $\rho_V / \rho_b = 180$ as a criterion to define “virialization”. If one takes into account the effect of the cosmological constant in the expansion of the background, and consider a flat universe ($\Omega_m + \Omega_\Lambda = 1$), the density contrast is given by (Bryan & Norman, ApJ 495, 80, 1998)

$$\Delta_V = \frac{\rho_V}{\rho_b} = 18\pi^2 + 82\left[\Omega_m(z_v) - 1\right] - 39\left[\Omega_m(z_v) - 1\right]^2 \qquad \text{IV.2.1.5}$$

where the density parameter Ω_m should be taken at the virialization redshift z_v In order to compute the phase space density indicator we need the mean density and the 1D velocity dispersion. The mean halo density at virialization is

$$\rho_V = \frac{3H_0^2\Omega_{m,0}}{8\pi G}(1 + z_v)^3 \Delta_v \qquad \text{IV.2.1.6}$$

On the other hand, since at virialization the 1D velocity dispersion satisfies the condition $3\sigma^2 = -2E$, one obtains (see details in Peirani & de Freitas Pacheco, arXiv:0701292)

$$\sigma^3 = \left[\frac{2}{3}\lambda^{-1/3} + \frac{1}{3}\lambda^{2/3}\right]^{3/2} \left(\Omega_\Lambda H_0^2\right)^{1/2} GM \qquad \text{IV.2.1.7}$$

where $\lambda = \Omega_\Lambda H_0^2 R_{max}^3 / GM$. Using also the result derived from simulations, i.e., the virialization redshift for a given halo of mass M is approximately given by

$$M_{11} = \frac{185}{\left(1+z_v\right)^{2.86}} \qquad \text{IV.2.1.8}$$

where M_{11} is the halo mass in units of 10^{11} M$_\odot$. From all these relations, one obtains finally for the phase space density indicator

$$Q \approx \frac{3.51\times10^{-9}}{M_{11}^{1.54}}\ \mathrm{M_\odot pc^{-3}km^{-3}s^{-3}} \qquad \text{IV.2.1.9}$$

The relation above represents the expected value derived from the spherical model of the phase space density indicator as a function of the halo mass just after virialization. This expression is compared (solid line) in figure 14 with data derived from the aforementioned simulations.

Figure 14
Predicted phase space density compared with simulated data

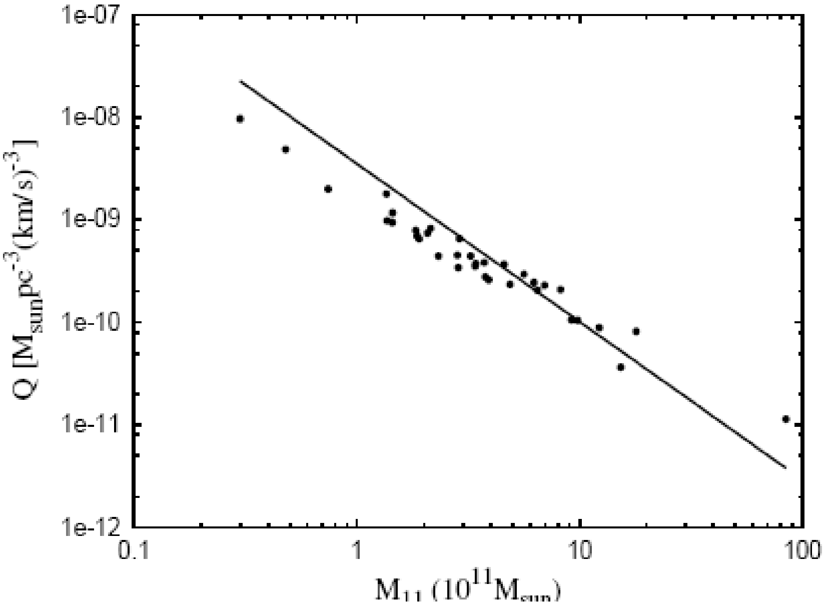

Notice that values of the phase space density indicator are several orders of magnitude smaller than those estimated at freezing of the abundance of dark matter particles. Such a reduction is due essentially to violent relaxation and phase mixing processes (to be discussed later), which lead the system to a quasi-equilibrium state.

After this dramatic reduction of the initial phase space density at shell crossing, halos continue to be assembled either by accretion through filaments or by mergers. These processes lead to a continuous decrease of the phase space density. This is illustrated in figure 15, where the evolution of the parameter *Q* is shown for a typical halo.

Another important information can be obtained from the correlation between *Q* and the central velocity dispersion of DM particles (both *Q* and σ_{1D} are computed inside a spherical volume with a radius equal to one tenth of the gravitational radius of the halo).

Figure 15
Evolution of the phase space density indicator *Q* derived from simulations

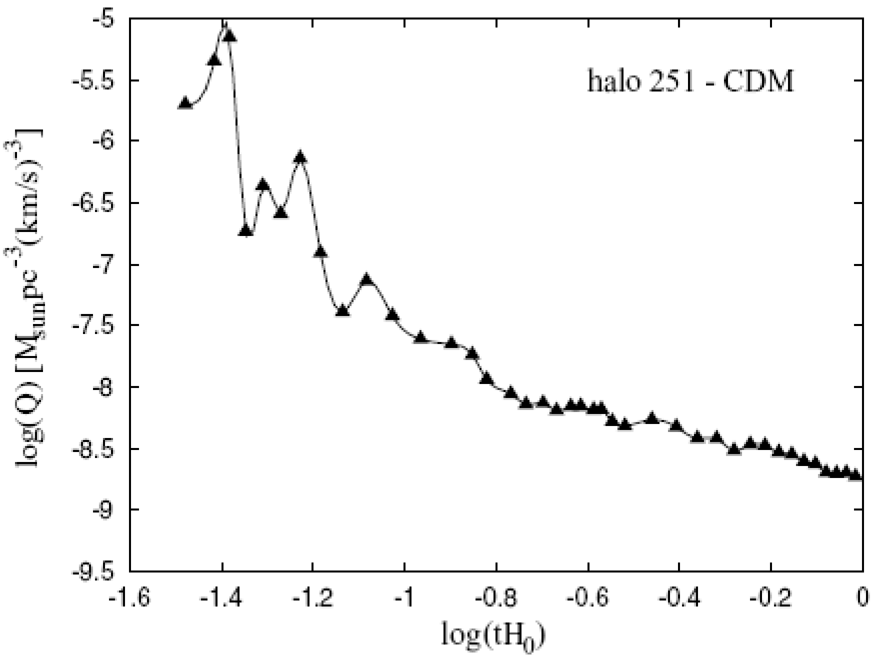

The observed slope of such a correlation is $d\lg Q/d\lg\sigma_{1D} = 2.65$ while simulations indicate a slope $d\lg Q/d\lg\sigma_{1D} = 2.16$. These results indicate that larger systems like clusters of galaxies have a lower phase space density than dwarf galaxies. This could be explained if clusters suffered different merger episodes (contrary of what has happened in the history of dwarf galaxies) that are able to reduce considerably the phase space density. The effect of mergers in the evolution of the density parameter can be seen in three examples shown in figure 17. The upper panels of the figure show the evolution of the derivative *dQ/dt* of the phase space density, while the lower panels show the corresponding variation of the velocity dispersion. In all the cases, the label 1 indicates the moment at which the shell crossing occurs. Notice that for each halo there is a peak in the derivative of the velocity dispersion and a valley in the derivative of *Q*. Thus, in the shell crossing phase, the transfer of energy from bulk to random motions increases the velocity dispersion and reduces the phase space density. The other events labeled 2, 3, …, correspond to merger episodes. In these episodes there is some heating produced by the violent relaxation mechanism (peaks in the derivative of the velocity dispersion) and a reduction of the phase space density (valleys in the derivative of the phase space density.

Despite these sudden variations of the phase space indicator during mergers, the relation $Q-\sigma_{1D}$ suggests that halos evolve in quasi-equilibrium. As the halo is assembled, its mass scales on the average with the central velocity dispersion as $M \propto \sigma_{1D}^{8/3}$. If, indeed halos evolve in quasi-equilibrium, the gravitational radius of the system evolves as $R \propto M/\sigma_{1D}^2 \propto \sigma_{1D}^{-2/3}$. Thus, $Q=\rho/\sigma_{1D}^3 \propto MR^{-3}\sigma_{1D}^{-3} \propto \sigma_{1D}^{-7/3}$, which is essentially the slope derived from simulations. These simulations demonstrate that the formation of structures and their late evolution define the value of Q at the present time.

Figure 17
The evolution of the derivative of the phase space density indicator (upper panels) compared with the evolution of the derivative of the velocity dispersion (lower panels) for three simulated halos.

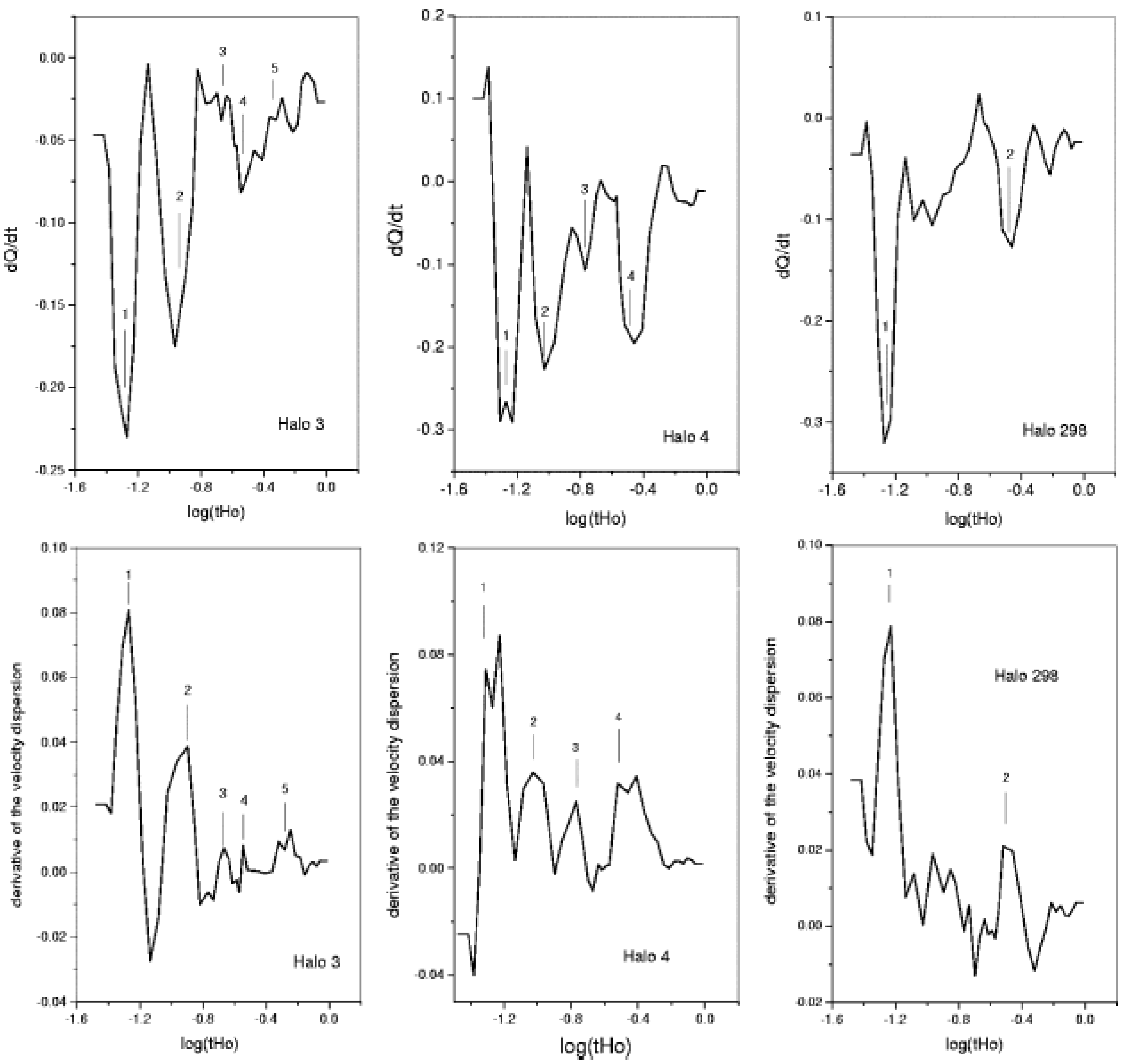

IV.2.2 Phase Space Mixing

Processes of mixing in phase space are generally due to non-local large scale dynamics, occurring far from equilibrium but promoting such a state. The process of mixing can be seen during merger events when significant variations of the gravitational potential occur. Here we consider the example of a main halo whose mass is about 4.0×10^{12} $M_\odot$ and the 1D central velocity dispersion is 202 km/s, which captures two satellites in eccentric orbits that will be disrupted by tidal forces. Satellite-1 has a mass of 1.6×10^{11} $M_\odot$ and a 1D central velocity dispersion of 51 km/s and satellite-2 has a mass of 2.8×10^{11} $M_\odot$ and a 1D central velocity dispersion of 78 km/s. The first sub-halo has an orbital period of about 6 Gyr and a periastron of about 100 kpc whereas the second sub-halo has a shorter period, namely, ~ 2 Gyr. In figure 18 are shown different snapshots of the evolution in the phase space diagram including as coordinates the radial velocity component of the particle and its radial distance to the center of the halo.

Figure 18
Phase space evolution of the capture of two sub-halos

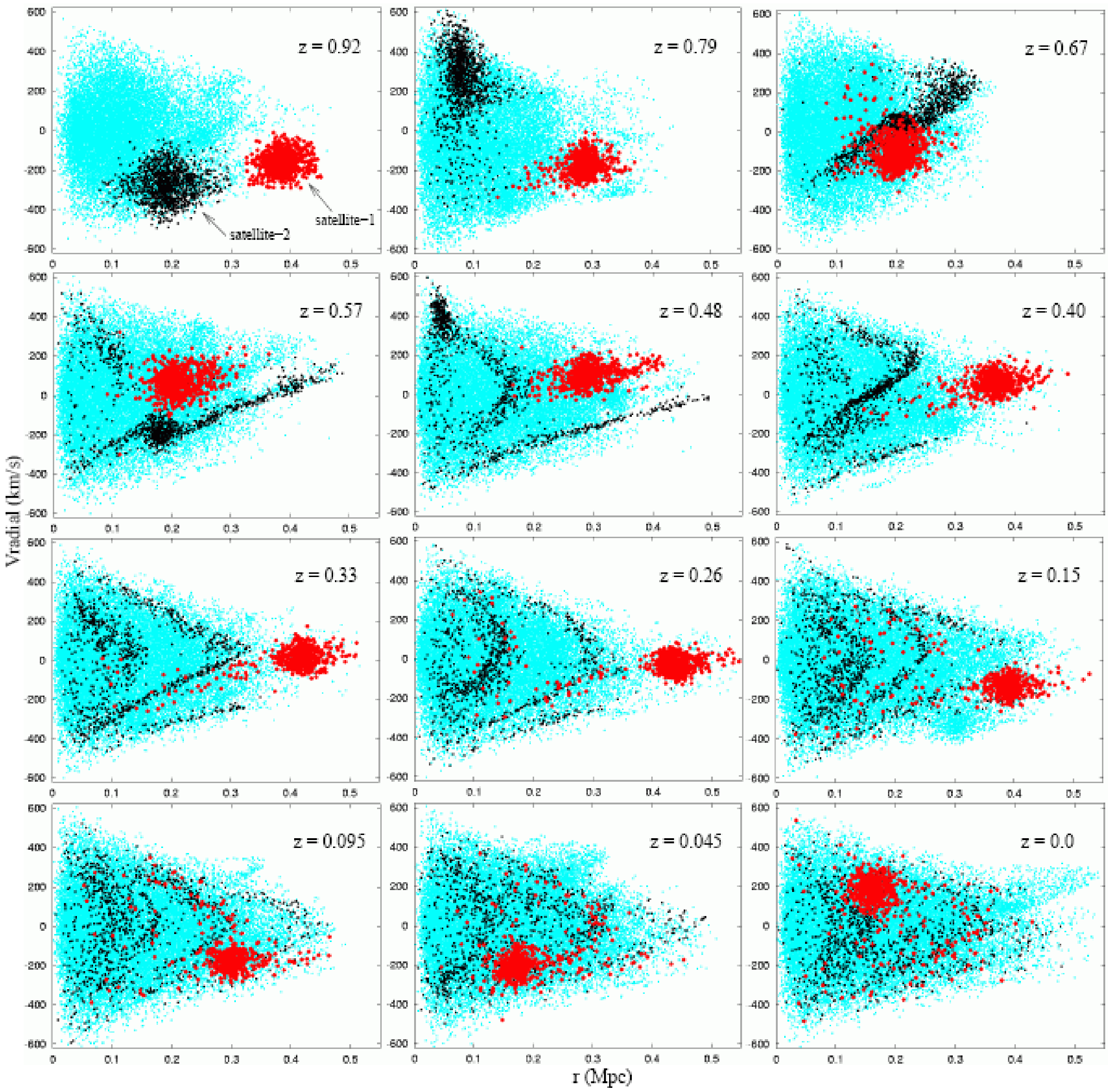

For each panel of figure 18, the corresponding redshift is indicated. Satellite-2 is completely disrupted after two periastron passages while satellite-1 passes to far from the center of the main halo to be disrupted, although it loses a significant amount of mass from its external regions. Notice that structures in phase space are gradually formed as satellite-2 passes by periastron. The observed streams in phase-space are similar to those derived from models of halo formation by secondary infall (Sikivie et al., PRD 56, 1863, 1997). However, in that case, structures are associated to “caustics” (mathematical surfaces of “infinite” density associated to cold collisionless particles). In real physical systems the density is limited by the fact that the motion of DM particles is not purely radial and that the velocity dispersion is finite and not zero. In a given instant and for a fixed value of the radial distance, a certain number of velocity peaks, corresponding to different streams can be seen in figure 18, which depend on the initial angular momentum. In the extreme limit of circular orbits, only one stream should be observed, as it occurs for satellite-1. The width of the m-velocity peak associated to the m-caustic is generally estimated from the Liouville theorem. In figure 19 are shown for the same snapshots, the evolution of the different radial velocity distributions.

Figure 19

Evolution of the radial velocity distribution for the main halo and satellites

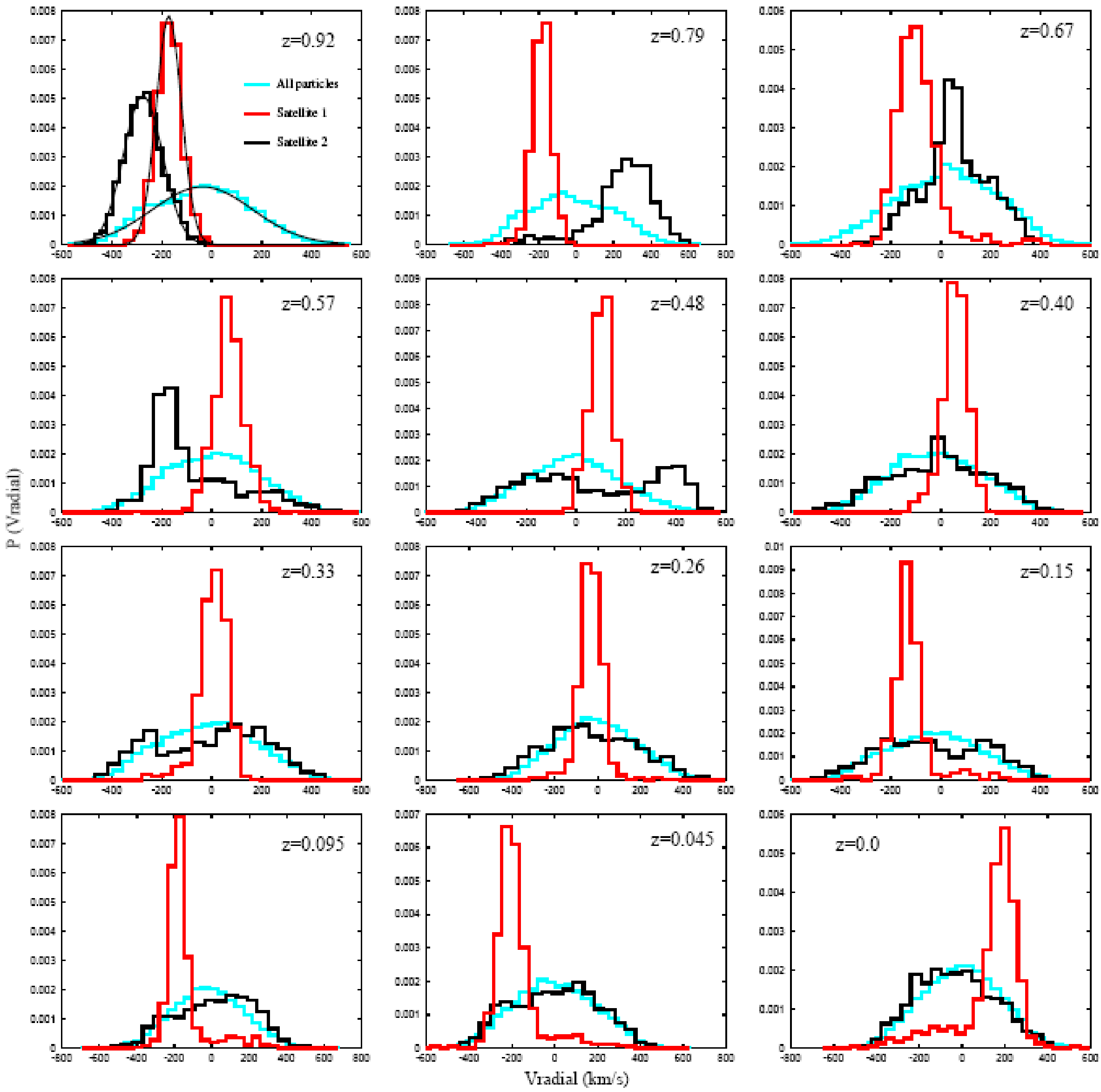

In the first snapshot of fig.19 (z = 0.92) it is possible to distinguish three distinct distributions associated to the main halo and to the two satellites. Despite satellite-1 to have preserved its identity, stripped particles from its outskirts mix in the velocity space. Notice in particular the appearance of extended tails in the velocity distribution of satellite-1, while the velocity distribution of satellite-2 coincides practically with that of the main halo after 3.5 Gyr due to an efficient mixing in phase-space. The "heating" process is probably due to tidal shocks. In spite of Gaussians be able to fit the radial velocity distribution of the main halo and sub-halos, the normalized kurtosis of these Gaussians is negative (κ =-0.57 for the main halo and κ =-0.73 for satellite-2), indicating that the radial velocity distributions have top-flatted profiles, with the effect being more accentuated in substructures.

Another interesting example concerns the fusion at z = 0.92 of two halos having respectively masses equal to $4.3\times10^{12}\,M_{\odot}$ and $1.2\times10^{12}\,M_{\odot}$ (see figure 20). Structures due to different periastron passages are still seen in phase-space at z = 0.48 but both objects are completely mixed at z = 0 (upper panels of figure 20). In the second row, panels show for the same redshifts the evolution of the radial velocity distribution for all particles constituting both halos and that of the sub-halo. Notice that at z = 0.92 the satellite is distinguishable, having a flat-topped Gaussian with a velocity dispersion of 131 Km/s. At z = 0.48, despite the presence of structures in phase space, both velocity distributions practically coincide, having a velocity dispersion of 251 Km/s. Such an increase or "heating" is probably due to tidal shocks as already mentioned. At z = 0, when structures have disappeared, the velocity distributions are indistinguishable from each other and a small "cooling", due to such a mixing, is noticed since the velocity dispersion of the "absorbed" halo is 237 Km/s.

Panels in the third and fourth rows show respectively the radial velocity distribution for all particles and for the sub-halo only in spherical shells at different radial distances. The distributions are well fitted by Gaussians having decreasing velocity dispersions as one should expect. This result contradicts the study by Wojtak et al. (MNRAS 361, L1, 2005), who concluded that out of the central regions halos do not have Gaussian velocity distributions.

IV.2.3 The Angular Momentum of Halos

Since the work of Fred Hoyle (MNRAS 109, 365, 1949), different studies addressed to the origin of the angular momentum of galaxies consider tidal interactions as the basic mechanism. As the protogalaxy (or protohalo) expands, its angular momentum grows almost linearly with time due to tidal interactions with their surroundings. The tidal mechanism ceases to be effective once the protohalo decouples from the expanding background, turns around and collapses. Hence, the turn around marks the instant of maximum angular momentum acquisition by the protohalo. The acquired angular momentum by this mechanism in the linear theory and under the Zeldovich approximation is

$$J_i = a^2 \frac{dD(t)}{dt} \varepsilon_{ijk} Q_{jl} I_{lk} \qquad \text{IV.2.3.1}$$

where *a* is the scale factor, *D(t)* is the linear growth factor, Q_{jl} is the deformation tensor that depends on the nearby distribution of matter and I_{lk} is the inertia tensor of matter inside the density perturbation volume. The tidal torques are non-zero only if the main axes of inertia are not aligned with the principal axes of the deformation tensor. In an Einstein-de Sitter universe, $J \propto t$ until maximum expansion.

Figure 20
Evolution in phase-space and of radial velocity distributions

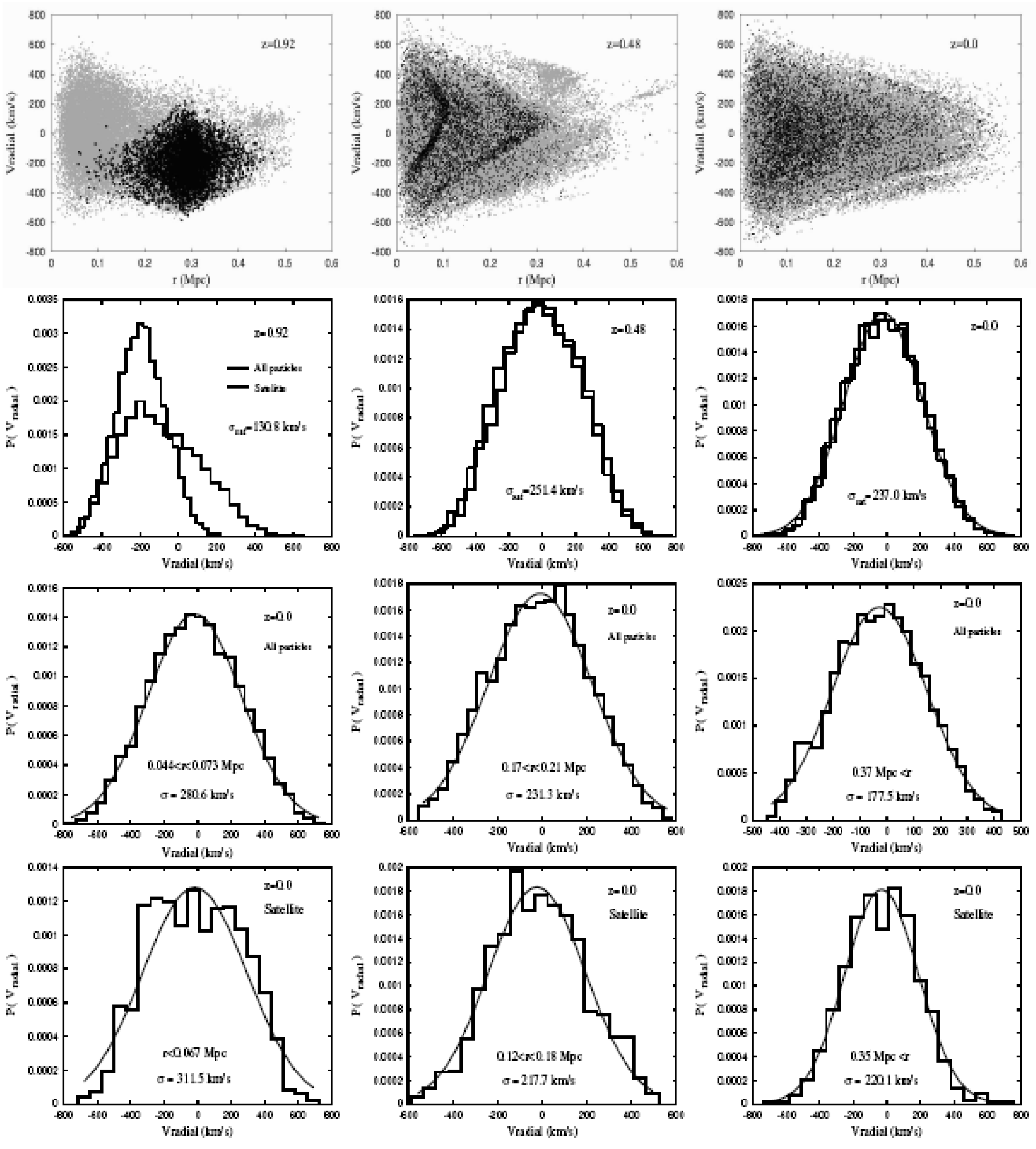

In the hierarchical scenario, small lumps of matter collapse first but accretion and merger effects modify the epoch of the maximum expansion with respect to predictions of the spherical model. Thus, the maximum angular momentum acquired by halos depends on their growth histories. Using the tidal linear theory one obtains for the ensemble average of the angular momentum (Catelan & Theuns, MNRAS 282, 455, 1996)

$$\left\langle J^2 \right\rangle^{1/2} = 7.4 \times 10^{65} (1 + z_{\max})^{-1/2} M_{11}^{5/3}\, kg\, m^2\, s^{-1} \qquad \text{IV.2.3.2}$$

where $z_{\max}$ is the redshift of maximum expansion and M_{11} is the halo mass in units of$10^{11}\,M_\odot$.

To fix the ideas, lets us first consider the case of our Galaxy, the Milky Way. The original data by Fall (IAU Symposium 71, 1983, p.391) on the angular momentum of spiral galaxies was recently revised and, from these data one obtains the fit

$$J_d = 7.3\times 10^{49} M_d^{1.57}\, kg\, m^2 s^{-1} \qquad \text{IV.2.3.3}$$

where the (baryonic) disk mass is in solar units. The mass of the disk of the Galaxy is not well known but a value around $4.0\times 10^{10}\,M_\odot$ seems reasonable. Similarly, estimates for the mass of our halo are uncertain but dynamical estimates lead to values of the order of $1.5\times 10^{12}\,M_\odot$ (see next section). Notice that these numbers imply a baryon-to-dark matter ratio lower than the cosmic value. Using the adopted value for the disk mass and the equation IV.2.3.3, one obtains for the specific angular momentum of the galactic disk $J_d / M_d \approx 4.0\times 10^{25}\, m^2 s^{-1}$. Using the results of Section IV.2.1, the redshift of maximum expansion for our halo is $z_{\max} \sim 2.9$. Then, using equation IV.2.3.2 one obtains for the specific angular momentum of the halo $J_h / M_h = 1.2\times 10^{25}\, m^2 s^{-1}$. Most theories of galaxy formation assume that the specific angular momentum of baryons and dark matter are equal. If this is the case then, taking into account the uncertainties in the masses, the linear tidal theory predicts a value about a factor 3-4 less than observations indicate. The situation would be worse had we assumed a cosmic baryon-to-dark matter ratio. If we wish to study non-linear effects, then cosmological simulations are needed. In fact, numerical experiments on the formation of galaxies indicate difficulties to produce galaxies with disks large enough (Steinmetz & Navarro, ApJ 513, 555, 1999). Simulated disks have, in general, less angular momentum than halos in the inner regions and miss high J-values observed in the halo J-distribution. On the other hand, Bullock et al. (ApJ 555, 240, 2001) claim, based on their simulations, that disks may have a “universal” angular momentum distribution. However, such a distribution is unable to produce “exponential” disks.

Based on semi-analytical models, Vitvitska et al. (ApJ 581, 799, 2002), considered an alternative scenario, namely, the spin of halos is built up gradually and randomly by accretion and mergers. Peirani et al. (MNRAS 348, 921, 2004) have investigated such a scenario using cosmological simulations as a tool. The follow up of individual halos has shown a strong correlation between the mass accretion rate and the variation rate of the angular momentum. The latter could be positive or negative according to the sense of the accreting flow with respect to the halo spin or, in case of mergers, according to the relative orientation of the spin and the orbital angular momentum. This is shown in figure 21.

Figure 21
Upper panels – variation of the accretion rate for two halos
Lower panels – variation of the angular momentum for the same halos

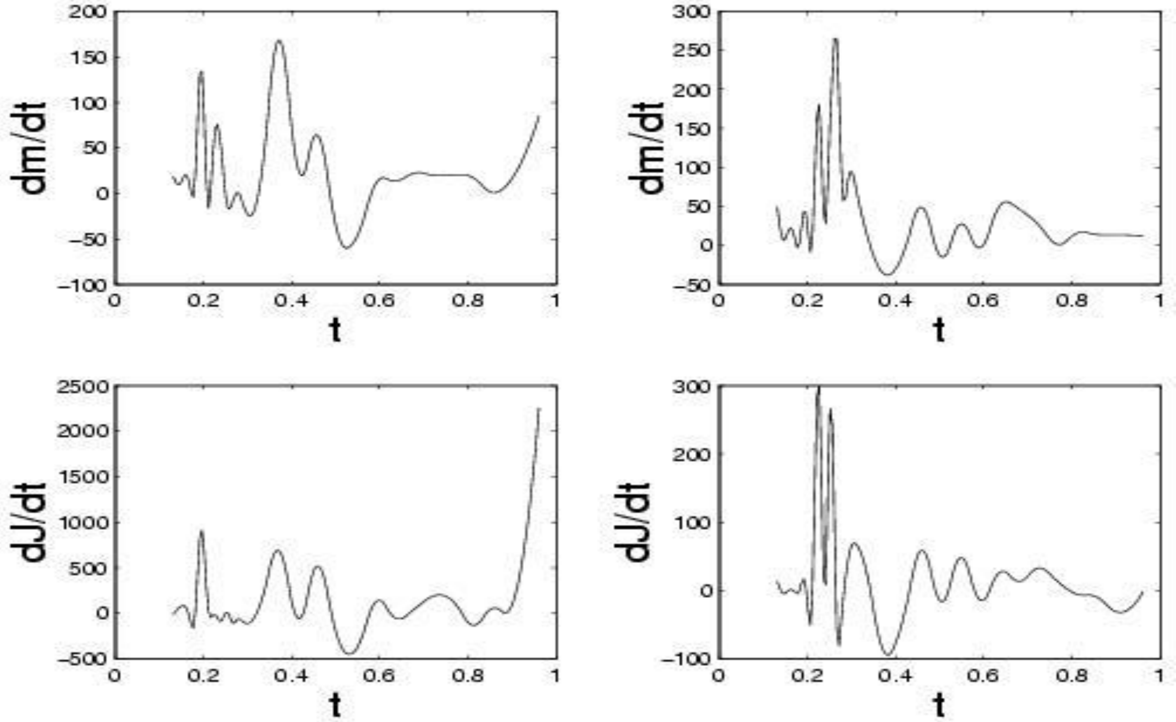

The acquisition of angular momentum by halos during accretion phases and merger episodes is also clearly demonstrated by figure 22, in which it can be seen the evolution of the median of the angular momentum distribution for halos that have grown either by accretion only or by important merger events.

Figure 22
Evolution of the angular momentum of halos

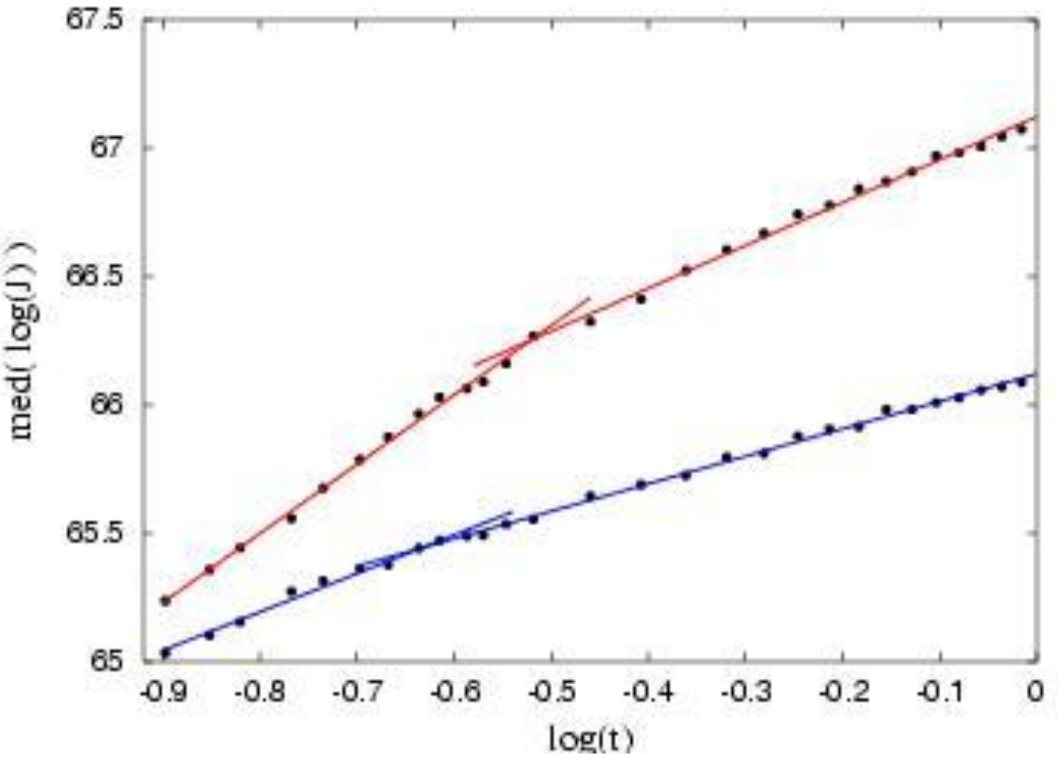

In figure 22, the upper curve corresponds to halos of the “merger class” while the lower curve corresponds to halos of the “accretion class”. Notice that halos of the former have presently an angular momentum almost one order of magnitude higher than halos of the latter class. Contrary to the tidal linear theory that predicts a linear growth of the angular momentum up to maximum expansion, cosmological simulations indicate a more rapid growth, i.e., $J \propto t^q$ where for halos of the “merger class”, q = 2.7 if z > 1.5 and q = 1.67 if z < 1.5, whereas for halos of the “accretion class”, q = 1.5 for z > 1.8 and q = 1.07 for z < 1.8 (the same regimes seen in the assembly of halos and in the total energy evolution). Moreover, the angular momentum of halos continue to grow even after the maximum expansion epoch, thanks to the transfer of the orbital angular momentum to the spin during a fusion episode or to the transfer of angular momentum of the accreted flow originated in filaments of the cosmic web.

V. The “coldness” of the Hubble flow

Using data from the CfA redshift survey, Davis & Peebles (ApJ 267, 465, 1983) derived for the r.m.s. of the velocity difference in the line-of-sight of correlated pairs, separated by less than 1 Mpc the value of 340 Km/s. However, from a sample of E-galaxies, Bruno & de Freitas Pacheco (ASP Conf.Series 24, 173, 1992) derived for their random motions a 1D velocity dispersion of 187 Km/s, in agreement with the previous estimate of Hale-Sutton et al. (MNRAS 237, 569, 1989), i.e., 167 Km/s. These values are significantly higher than the 1D velocity dispersion found by Sandage et al. (ApJ 172, 253, 1972) for the local Hubble flow (*R* < 2-4 Mpc), i.e., 60 Km/s. This result motivated those authors to conclude that the local flow is relatively “quiet” and “cold”. Further analyses revealed even lower values ~ 30 Km/s (Ekholm et al., A&A 368, L17, 2001; Karachentsev et al., A&A 389, 812, 2002). The 1D velocity dispersion seems to increase slightly with the radius *R* of the local volume since Karachentsev et al. (A&A 398, 479, 2003) found a velocity dispersion of about 85 Km/s for R≤5.5 Mpc while Tikhonov & Kyplin (MNRAS 395, 1915, 2009) found 97 Km/s for R≤7.0 Mpc. The latter results are consistent with the conclusions by Maccio et al. (MNRAS 359, 941, 2005), who derived the following expression for the 1D velocity dispersion

$$\sigma_H = (88 \pm 20) \times (R/7Mpc) \;\; Km/s \qquad \text{V.1}$$

Different explanations have been proposed to understand the “coldness” of the local flow and, in particular, the possible effects of the cosmological constant. However, different cosmological simulations **including Λ**, disprove such an idea: Governato et al. (New Ast. 2, 91, 1997) obtained $\sigma_H = 150 - 300\,Km/s$, Peirani & de Freitas Pacheco (New Ast. 11, 325, 2006) derived $\sigma_H = 73\,Km/s$, in good agreement with the simulations by Maccio et al. (MNRAS 359, 941, 2005), who obtained a 1D velocity dispersion of 80 Km/s within a local volume of radius 3 Mpc.

More recently, this question was reviewed by Martinez-Vaquero et al. (MNRAS 397, 2070, 2009), who performed new N-body simulations of the local universe. These authors found that world models including or not a cosmological constant have similar values of σ_H that excludes Λ as the cause or main cause of the “coldness” of the flow. However, Martinez-Vaquero et al. obtained an interesting result from their simulations: σ_H correlates with the mean matter density of the local volume (radius of 7 Mpc in their case) normalized by the mean cosmological density. A totally different approach was considered by Aragon-Calvo et al. (MNRAS 415, L16, 2011). In their scenario, the "coldness" is a consequence of the geometry and dynamics of our local wall. The expansion of the local wall also affects the measurement of the local Hubble constant and, in the range 1 < R < 3 Mpc, according to their simulations, the expected 1D velocity dispersion should be around 30 Km/s.

In general, the 1D velocity dispersion with respect to the Hubble flow is computed from the relation

$$\sigma_H^2 = \frac{1}{N}\sum_{i=1}^{N}\left(V_i - H_0 r_i\right)^2 \qquad \text{V.2}$$

where V_i and r_i are respectively the radial velocity and the radial distance to the center of mass of the Local Group of a given satellite. In reality, nearby satellites have negative velocities since they feel the gravitational effects of the MW-M31 pair and only beyond a certain distance they follow a "pure" Hubble flow. Thus, in our approach, the 1D velocity distance will be computed from the relation

$$\sigma_H^2 = \frac{1}{N}\sum_{i=1}^{N}\left[V_i(r) - V_{TL}(r)\right]^2 \qquad \text{V.3}$$

Here we follow Peirani & de Freitas Pacheco (New Ast. 11, 325 2006 and A&A 488, 845, 2008), assuming that the velocity profile near the Local Group is given by the Tolman-Lemaître spherical model, including the contribution of the cosmological constant. Inside the "zero"-velocity surface satellites are collapsing and therefore have negative velocities, outside they have positive velocities but are gravitationally bound (they will reach maximum expansion in the future and then collapse) and beyond the "zero"-energy surface, they follow a pure Hubble flow. From the numerical solution of the equations of motion, they have obtained the velocity profile

$$V_{TL}(r) = -\frac{0.976}{r^n}\left(\frac{GM}{H_0^2}\right)^{(n+1)/3} + 1.377 H_0 r \qquad \text{V.4}$$

where $n = 0.627$ and M is the total mass of the Local Group (MW+M31). The "zero"-velocity surface can be estimated from the above equation from the condition $V_{TL}(R_0) = 0$. Expressing the result in terms of the mass, one obtains

$$M = 1.89\frac{H_0^2 R_0^3}{G} \qquad \text{V.5}$$

Thus, if the radius R_0 of the "zero"-velocity surface can be estimated from observations of the velocity profile, the mass of the system can be derived. Notice that the radius R_E of the "zero"-energy surface satisfies the condition $V_{TL}(R_E) = H_0 R_E$ and one can easily show that $R_E = 2.217 R_0$. Using this approach, Peirani & de Freitas Pacheco (A&A 488, 845, 2008) derived the 1D velocity dispersion for several systems in the local universe, listed in table 1.

Table 1
Groups in the Local Universe

Group	**MW/M31**	**M81**	**NGC 253**	**IC 342**	**CenA/M83**
$\sigma_H (Km/s)$	**36**	**53**	**45**	**34**	**45**
$M(10^{12}\,\mathrm{M}_\odot)$	3.0 ± 0.8	0.92 ± 0.24	0.13 ± 0.18	0.20 ± 0.13	2.1 ± 0.5

Notice that the "coldness" is observed not only for the pair MW-M31 but also for the groups M81, NGC 253, IC 342 and CenA-M83.

Suppose that these groups are represented by density fluctuations above the background having a Gaussian profile, namely

$$\delta_f(r) = A\exp\left(-\frac{r^2}{2R^2}\right) \qquad \text{V.6}$$

where A is a normalization constant, which can be obtained from the condition that the total mass of the perturbation is

$$M = \int_0^\infty \delta_f(r)\rho_b d^3r \qquad \text{V.7}$$

From eqs. V.6 and V.7 one obtains

$$A = \frac{M}{\left(2\pi^3\right)\rho_b R^3} \qquad \text{V.8}$$

Compute now the Fourier transform of V.6, i.e.,

$$\delta_f(k) = \int \delta_f(r)\exp\left(-i\vec{k}\cdot\vec{r}\right)d^3r = \frac{M}{8\pi^{3/2}\rho_b}\exp\left(-\frac{k^2R^2}{4}\right) \qquad \text{V.9}$$

On the other hand, in the linear approximation, the Fourier component of the peculiar velocity is given by

$$\vec{V}(k) = -\frac{Ha}{ik^2}\left(\frac{\partial \lg D}{\partial \lg a}\right)\delta_f(k)\vec{k} \qquad \text{V.10}$$

where a is the scale factor and D is the growing mode of the linear density fluctuation. From Parseval's theorem, the mean square velocity within a volume V_* is

$$\left\langle V_p^2 \right\rangle = \frac{1}{V_*}\int \left|V^2(k)\right| d^3k \qquad \text{V.11}$$

Plugging eqs. V.9 and V.10 into eq. V.11 one obtains

$$\left\langle V_p^2 \right\rangle = \frac{1}{16\sqrt{2\pi^3}} \frac{(Ha)^2}{V_* R} \left(\frac{\partial \lg D}{\partial \lg a} \right)^2 \frac{M^2}{\rho_b^2} \qquad \text{V.12}$$

Now, fix the parameter R by imposing that 90% of the total mass is included within a sphere of radius r_* (for instance, in the case of the MW-M31 pair, this is about 1 Mpc). Thus, $R = 2r_*/5$. Recalling that the mean matter density inside the volume V_*, where the mean velocity dispersion is computed is $\bar{\rho} = M/V_* = 3M/4\pi r^3$, one obtains finally for the mean square peculiar velocity

$$\left\langle V_p^2 \right\rangle^{1/2} = \frac{\sqrt{10}}{(4608\pi)^{1/4}} (Hra) \left(\frac{\partial \lg D}{\partial \lg a} \right) \left(\frac{r}{r_*} \right)^{1/2} \left(\frac{\bar{\rho}}{\rho_b} \right) \qquad \text{V.13}$$

Notice that the present (a = 1) 1D-velocity dispersion is (case of isotropic peculiar motion) $\sigma_H = \left\langle V_p^2 \right\rangle^{1/2} / \sqrt{3}$. Thus

$$\sigma_H = 0.167 f(\Omega_m)(H_0 r) \left(\frac{r}{r_*} \right)^{1/2} \left(\frac{\bar{\rho}}{\rho_b} \right) \qquad \text{V.14}$$

Within a spherical volume of radius r = 2.5 Mpc (about the radius of the “zero”-energy surface for the Local Group) and $r_* = 1 Mpc$, one obtains from the equation above $\sigma_H = 23(\bar{\rho}/\rho_b)$ Km/s. The matter overdensity in such a volume due to the pair MW-M31 is about 1.3, implying $\sigma_H = 30$ Km/s , in good agreement with the derived value (see table 1).

VI. Main conclusions

Up to the present date, there is no convincing evidence from direct or indirect experiments for the existence of dark matter. Despite negative results from the LHC concerning supersymmetry, the possible detection of the scalar Higgs boson with a mass around 125 GeV points to a minimum mass around 160 GeV for the lightest supersymmetric particle. This is consistent with the non-detection of γ-rays originated from M87, either at energies of 100 MeV or 1 GeV by Fermi-LAT. A possible annihilation γ-ray line at 130 GeV is also consistent with these figures.

Dark matter manifests via gravitational effects at different scales: clusters of galaxies (~ 2 Mpc), groups of galaxies (100-400 Kpc), binary galaxies (~ 50 Kpc), galaxies themselves (~ 20 Kpc) and in the solar neighborhood (~ 1 Kpc).

The structures present in the universe are formed hierarchically by fusion of small lumps of dark matter, whose minimal mass is around 10^4 $M_\odot$, if the mass of particles is around 100-200 GeV. As halos are assembled either by accretion or mergers, the core density decreases on the average, by one order of magnitude in the redshift interval $10 < z \leq 0$.

The inner regions of the lumps of matter collapse first and, in this shell crossing phase, a rapid transfer of energy from bulk to random motions occur, leading to a rapid increase of the velocity dispersion and a decrease in the phase-space density. This early evolutionary phase is followed by a late period of “slow” heating. Simulations indicate that the energy transfer from bulk to random motions produces a heating of all particles regardless their initial energies. Halos issued from simulations with particles of different masses relax according to predictions of the violent relaxation mechanism, i.e., at the end all particles have the very same velocity dispersion. This relaxation process leads to a flat-topped velocity distribution.

In the process of accretion and/or during merger episodes, halos acquire angular momentum. The growth of angular momentum during the assembly of halos is faster than that due to tidal torques, which is operative only up to the phase of maximum expansion of lumps.